Digital accelerometry: A possible clinical technique for the evaluation of osteoarthritis of the knee joint

by

Anqi Zhang

A Thesis Submitted to the

Graduate Faculty in Partial Fulfillment of the

Requirements for the Degree of

MASTER OF SCIENCE

Departments: Biomedical Engineering
Electrical Engineering and Computer Engineering
Co-majors: Biomedical Engineering
Electrical Engineering

Approved:

Signatures have been redacted for privacy

Iowa State University
Ames, Iowa
1988

TABLE OF CONTENTS

LIST OF FIGURES

LIST OF TABLES

1 INTRODUCTION

Arthritis is the nation's most crippling disease threatening millions of Americans. Of the many types, osteoarthritis is most common. Osteoarthritis is a degenerative joint disease probably resulting from aging and is most likely to affect joints, such as the knee and the lower portion of the vertebral column, which receive the greatest abuse over the years. The process usually starts with the hardening of the subchondral bones followed by gradual softening and disintegration of the articular cartilage in the joint.

Presently, clinical determination of osteoarthritis relies on procedures such as palpation, arthroscopy, biochemical studies, and X-rays. The fact that some of those techniques are either qualitative or invasive and others involve large capital investment or extensive training limits their clinical utilization. A simple technique is needed to quantitatively measure *in vivo* the pathological condition of the articular cartilage as a result of osteoarthritis.

Voloshin and Burger (1982) have employed an accelerometric technique in an attempt to characterize the vibration wave attenuation properties of the articular cartilage of the knee joint and to relate them to the arthritic conditions of the subject. The study presented here aimed to: provide a theoretical basis for the technique, extend it experimentally, and find its limitations concerning clinical uti-

lization.

The physiological phenomenon under consideration is the transient vibratory response of the human tibia and femur to an impulsive impact between the heel and a concrete floor in normal walking. A lightweight accelerometer was attached to the tibial lateral condyle and another to the femoral medial condyle using elastic straps. The accelerations of the tibia and femur resulting from heel strike of the subject walking barefooted were registered, stored, and later processed using a DEC PDP-11 computer. The transmissibility function, characteristic of the mechanical properties of the resilient element between the tibia and the femur, namely articular cartilage and surrounding subchondral bones of the knee, was calculated and plotted using the acceleration data.

An engineering model of the tibia-knee-femur system was presented to theoretically analyze the transient response of the tibia-knee-femur vibratory system to the heel strike in the normal gait. This model, though limited by restrictive assumptions, appeared useful, at least qualitatively, in characterizing mechanical properties of the articular cartilage and subchondral bones of the knee joint.

It was found that the characteristics of the transmissibility function could provide useful information on how the osteoarthritic condition of the knee joint progressed. The crosscorrelation function between the tibial and femoral transient acceleration responses to the heel strike also served to reveal the attenuation properties of the knee joint.

Although some problems with design of the accelerometers, effect of muscle tone and joint motion on the transmissibility, and reproducibility require further study, the noninvasive nature and simple procedure of the technique seem to hold high promise as a diagnostic tool for the degenerative disease in a clinical setting.

2 OBJECTIVES

The primary objective of the study was to assess the possibility of clinical usage of a digital accelerometric technique in documenting the progression and possible early detection of osteoarthritis in the knee joint. Specifically, goals were

- to derive an engineering model of the tibia-knee-femur system on which the experimental procedure could be based,
- to analyze and extend the technique to obtain results that would truly reveal the physiological characteristics of the articular cartilage of the knee joint, and
- to find limitations of the technique that would affect clinical utilization and the direction of future work.

3 LITERATURE REVIEW

3.1 Osteoarthritis

Osteoarthritis, or more descriptively degenerative joint disease, is a common finding in adults. X-rays show some evidence of osteoarthritis in at least one joint of most people age 40 or older. In the United States alone, 30 million people are estimated to suffer from osteoarthritis related pain, far more than people with all other forms of arthritis combined (Burfoot, 1986; Ruoff, 1986). Osteoarthritis develops most commonly in older people, in the larger, weight-bearing joints such as hips, knees, and spine. Though little is known about the causes of the disease at the present time, it is generally believed that the arthritic condition is worsened by every-day wear and tear on an already affected joint (Spence and Mason, 1983; Kunz and Finkel, 1987).

Osteoarthritis is a process of cartilage destruction manifested by slow wearing-away of articular cartilage eventually exposing smooth bone ends and leading to a painful joint (Marcinko and Dollard, 1986; Roberts *et al.*, 1986). No matter what the cause is, be it purely mechanical, biochemical, or a combination of both, the articular cartilage in osteoarthritis shows a loss of proteoglycans and a breakdown of the collagen fiber framework. As the disease progresses, the cartilage becomes more disintegrated, more extractable, softer in compression, and weaker in tension.

The end result is a total loss of the cartilage that leaves the two bone ends to come into contact and glide on each other, completely crippling the patient (Bihari-Varga *et al.*, 1984; Roberts *et al.*, 1986).

The constant mechanical wear and tear on the articular cartilage is believed to be compensated for by an active repairing process. In fact, studies done on rabbits have shown signs of chondrocyte regeneration and proteoglycan synthesis in the articular cartilage to which degenerative alterations had been induced by either mechanical stress or biochemical agents. Unfortunately, this reparative capacity is limited because of the lack of vascular networks needed to supply nourishment, and is also age dependent due to the slowing down of metabolism (Burfoot, 1986; Magdolna Bihari-Varga *et al.*, 1984; Marcinko and Dollard, 1986).

3.2 Diagnostic Techniques

X-ray examination is the primary clinical method for detecting degenerative joint disease *in vivo* (Chu *et al.*, 1978; Mollan *et al.*, 1983: Kunz and Finkel, 1987). Abnormalities of the articular cartilage shown on the x-ray film in conjunction with proper blood tests allow the physician to make an accurate diagnosis. Because of its low sensitivity, however, the procedure provides no early warning on the condition of the diseased articular cartilage but poses the risk of excessive radiation exposure to the subject. Moreover, interpretation of radiologic images is subjective and thus varies from physician to physician. Other methods, such as arthroscopy and open biopsy, provide a direct evaluation of the articular cartilage, but their value is diminished by their cost and the hazard they pose as invasive procedures.

In searching for a noninvasive clinical tool for objective evaluation of dam-

age to articular cartilage due to osteoarthritis, some researchers have used electro-acoustical techniques in an attempt to relate biomechanical factors of diseased joints to the degree of cartilage destruction (Chu *et al.*, 1978; Voloshin *et al.*, 1981; Voloshin and Burger, 1982; Voloshin and Wosk, 1983). Much of the early work has concentrated on the knee joint because of its size and susceptibility to the degenerative joint disease. Chu and his colleagues (1978, 1976) used microphones to acquire acoustic signals generated by the knee joint during active articulation. They found a shift in the power spectra of two sets of signals obtained two months apart on the same subject with a knee disorder, an indication of progressive lesion to the cartilage, as corroborated by arthroscopy.

Voloshin and Wosk (1983, 1982) were concerned with the attenuation ability of the knee joint to the intermittent forces as a result of heel strike. Viewing the articular cartilage between the tibia and femur as a natural absorber, they modeled the tibia, knee, and femur as a mechanical vibratory system in the course of heel strike, and used an accelerometric method to obtain vibrational transmissibility parameters of the knee that were related to clinical conditions of the articular cartilage.

3.3 Accelerometric Method

Accelerometry as a technique for the measurement of human bone vibrations has been investigated for many years (Morris, 1973; Nokes *et al.*, 1984; Ziegert and Lewis, 1979). Such methods involve the use of small accelerometers, either directly pinned onto the bone or strapped to the bone over the skin layer, to transduce bone acceleration due to some external force input. For purposes of analysis, other

vibrational parameters, such as velocity and displacement, can be readily calculated using the acceleration data.

Strictly speaking, an accelerometer has to be mounted directly to the bone in order for the resulting signal to be truly representative of the bone vibration. To determine the effect of the underlying skin, Light *et al.* (1980) firmly attached an accelerometer to the tibia of an investigator by driving two stiff pins through vertical slits in the skin into the tibia and compared the measurements with those recorded with another accelerometer strapped over the skin. Their results indicated that only high-frequency components were lost to a skin mounted transducer due to the soft tissue damping effect (Light *et al.*, 1980; Light and McLellan, 1977). More recent work has shown that the effect of the soft tissue between a skin mounted accelerometer and the bone could be minimized by choosing small mass accelerometers (Mollan *et al.*, 1983; Nokes *et al.*, 1984; Saha and Lakes, 1977; Ziegert and Lewis, 1979).

Voloshin and his co-workers (1984, 1983, 1981) applied the accelerometric technique to the evaluation of properties of the articular cartilage in the knee joint. When the subject walked barefooted, the longitudinal vibration transients generated as a result of heel strike were propagated through the skeleton and picked up by two lightweight accelerometers strapped to the tibial tuberosity below the knee and the femoral medial condyle above the knee. The transduced electrical signals were recorded in the time domain and analyzed in both the time and frequency domains to yield transmissibility parameters between the two anatomical aspects across the knee. They found that the difference between the two peak acceleration values from below and above the knee, shock absorbing capacity as they called it,

was correlated to the clinical condition of the knee joint.

Voloshin and Burger (1982) took a further step to define the transmissibility function of the knee joint as the ratio of the discrete Fourier transform of the acceleration of the femoral medial condyle to that of the tibial tuberosity. They hypothesized, without providing a theoretical basis, that the knee could be modeled as a simple two-degree-of-freedom rheological system and, as such, the transmissibility function was characteristic of the integrity of the joint.

3.4 Vibration Transients due to Heel Strike

Figure 3.1 plots the acceleration measurements as recorded in the present study by two accelerometers strapped, along the longitudinal axis of the leg, at two points across the knee joint of a barefoot walking subject. A complete gait cycle is defined to be between the two consecutive heel strikes and can be divided into three phases. The first, called loading or vibratory transient phase, starts at the instant of the heel strike and ends when the vibration is completely damped out. Following the vibrational transients is a stationary phase marked by a flat acceleration plot as the foot essentially remains on the floor. The completion of the cycle is a leg swing phase during which measurable accelerations are found. These are due to the movements of the leg raising, swinging forward, and dropping on the floor (Maquet, 1980)

The objective in determining the properties of the knee cartilage dictates the importance of the first phase. Upon an impact of the heel on the floor, the heel experiences an upward impulsive force with a duration of less than five milliseconds, a peak value of about 110 percent of the subject's body weight, and frequency components of up to 75 Hertz (Dickinson *et al.*, 1985; Folman *et al.*, 1986; Simon

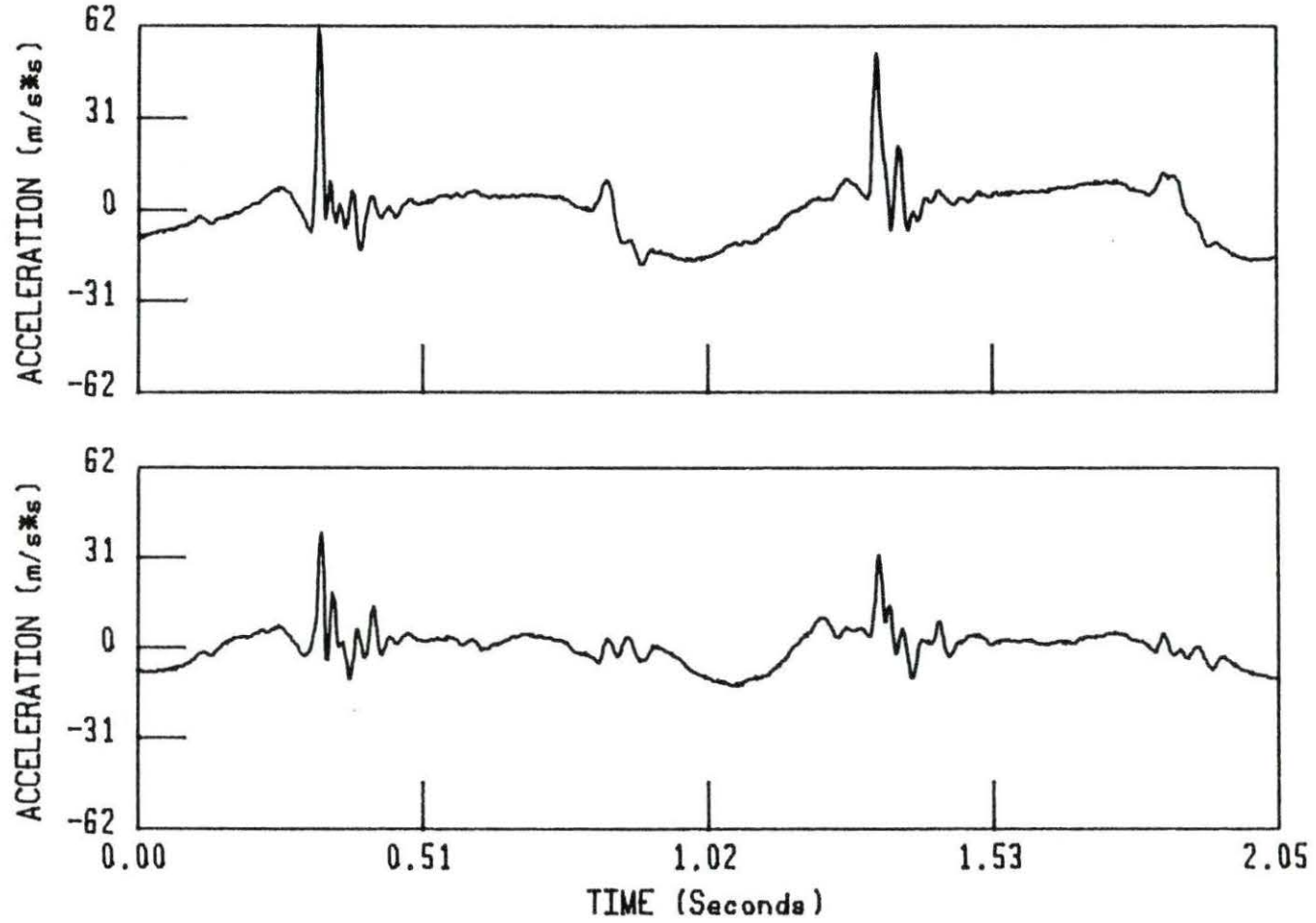

Figure 3.1: Acceleration measurements from the tibia and femur. Tibia–top plot; femur–bottom plot

et al., 1981). This high frequency impulsive loading at heel strike initiates brief but sizeable longitudinal vibration transients of the long bones such as the tibia and the femur. Those transitional vibration waves propagate along the skeletal system to as high as the skull and, at the same time, are moderated by the resilient elements such as the heel pad, articular cartilage, and subchondral bones (Radin and Paul, 1972; Simon *et al.*, 1972; Sokoloff, 1963).

3.5 Shock Absorption of Joints and Degenerative Joint Disease

One of the major functions of a weight-bearing joint is to absorb vertical shock waves transmitted through the skeletal system in every day activities (Folman *et al.*, 1986; Wosk and Voloshin, 1981). This shock absorption function is accomplished by resilient components such as cartilage, ligaments, muscles, cancellous subchondral bones, synovial capsule, and synovial fluid. The relative contribution of each component to the shock absorptive capacity is dependent on the mechanical properties as well as the orientation of the component.

A photographic view of the knee joint in Figure 3.2 with the overlying soft tissue cut shows the relative orientation of the various components of the joint. The cancellous subchondral bones are the end portions of the tibia and the femur. In a normal joint, the cancellous subchondral bone is most effective in absorbing cyclic longitudinal forces resulting from heel strike (Maquet, 1980; Radin and Paul, 1970). The subchondral bone offers shock absorption through mechanical deformation. The fluid-filled articular cartilage, on the other hand, contributes little to shock absorption due to its viscoelastic nature. Deformation of the cartilage is difficult because fluid is bound to both collagen and the proteoglycan component of the

cartilage (Marcinko and Dollard, 1986). Only by squeezing the cartilage slowly will enough fluid flow out to allow for significant deformation.

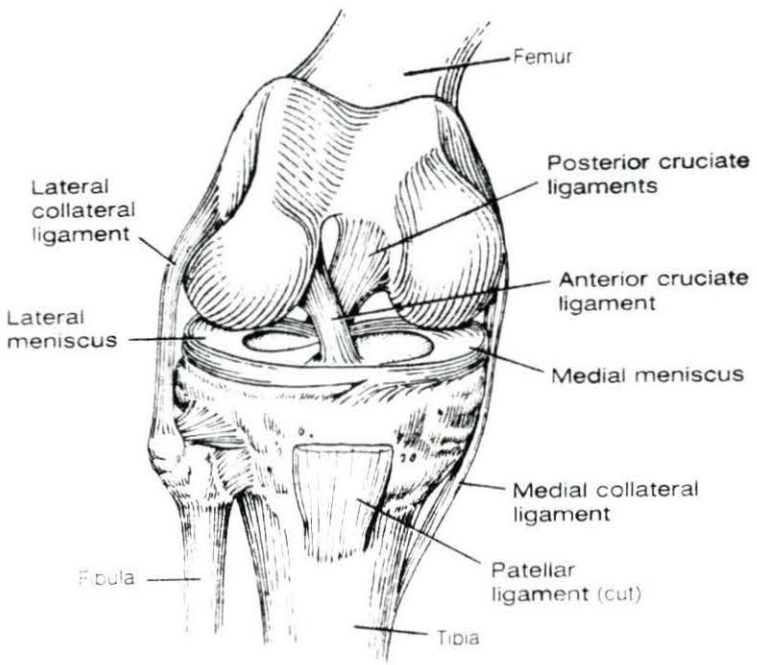

Figure 3.2: Knee joint with the soft tissue cut. Meniscus–special name for the articular cartilage of the knee joint

Experimental evidence has shown that cyclic impacts between the heel pad and the floor in walking accelerated the wearing-out process of the articular cartilage (Radin *et al.*, 1978; Simon *et al.*, 1972). If the cartilage renders little deformation to absorb vertical shock waves, how then does repetitive loading contribute to the cartilage degeneration? This led Radin and Paul (1972) to hypothesize that the repetitive vertical impact loading would, over time, cause a change in the resilient

structure of the subchondral bone leaving the articular cartilage unprotected from the impact forces during heel strike. This would increase the stress on the cartilage and thus facilitate the degeneration process. Their theory was echoed by later studies that found subchondral sclerosis in patients in early stages of osteoarthritis (Maquet, 1980; Roberts *et al.*, 1986).

The increased stiffness of the subchondral bone is believed to be due to the healing process of trabecular microfractures caused by the impact loading. Some studies of the subchondral bone by micrography (Little and Pimm, 1958; Radin and Paul, 1970; Simon *et al.*, 1972) have demonstrated trabecular microfractures in the subchondral bones of animals subjected to repetitive impulsive loading, and others (Dekel and Weissman 1978; Roberts *et al.*, 1986) have shown presence of healing or healed trabecular microfractures in the subchondral bone of patients in early stages of joint degeneration.

Ligaments, capsule, synovial tissue, and synovial fluid have been found to contribute little to the shock absorption (Paul *et al.*, 1978). Whether active muscle contraction plays any role in absorbing the shock waves transmitted to the skeletal system is still subject to debate. The muscle tissue itself without contraction has been shown to have no absorption effect (Paul *et al.*, 1978). Since muscle reaction time is on the order of 75 milliseconds, the only mechanism with which muscle could act to attenuate the incoming peak dynamic forces would seem to be preprogramming the muscle to anticipate the incoming waves.

4 THEORETICAL CONSIDERATIONS

If the assertion that the transmissibility function defined in the previous section is characteristic of mechanical properties of the articular cartilage and the subchondral bones of the knee joint under test is true, then, because of the interrelationship between their mechanical properties and osteoarthritis, one can assess the osteoarthritic condition of the knee joint using the transmissibility function. This section is intended to present an idealized engineering model of the knee which will enable one to check the validity of the claim.

4.1 Transmissibility of a Translational System in Velocity Shock

Consider a two-degree-of-freedom linear translational system subjected to a sudden change in velocity, termed velocity shock. As shown in Figure 4.1, m_1 and m_2 represent two masses on a frictionless surface. k_1 and k_2 are spring constants, and c_1 and c_2 viscous damping coefficients. The entire system moving to the right strikes a fixed support with its right end at velocity v_0, with $t = 0$ at the time of impact. The reference coordinate systems for displacement are so chosen that the initial displacements of the two masses are zero. It is desired to find the ratio of transient accelerations of the two masses as a function of radial frequency ω.

In reference to the free body diagram also shown in Figure 4.1, application of

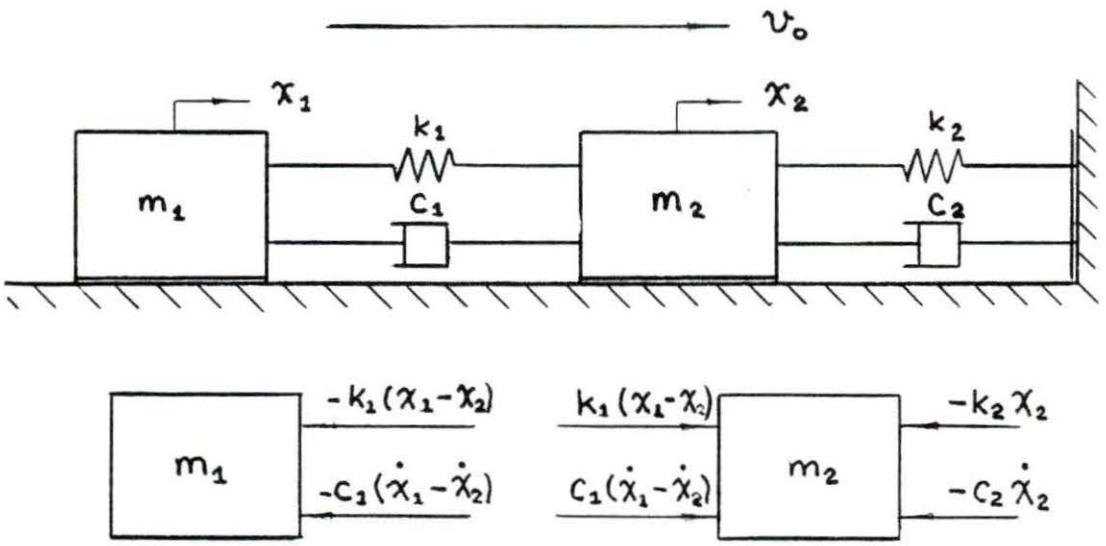

Figure 4.1: A two-degree-freedom system in velocity shock and its free-body diagram

the Newton's second law gives the system equations of the motion

$$\begin{aligned} m_1\ddot{x}_1 + c_1(\dot{x}_1 - \dot{x}_2) + k_1(x_1 - x_2) &= 0 \\ m_2\ddot{x}_2 + c_2\dot{x}_2 + k_2x_2 - c_1(\dot{x}_1 - \dot{x}_2) - k_1(x_1 - x_2) &= 0 \end{aligned}$$

or, after rearranging,

$$\begin{aligned} m_1\ddot{x}_1 + c_1\dot{x}_1 + k_1x_1 - c_1\dot{x}_2 - k_1x_2 &= 0 \\ m_2\ddot{x}_2 + c_2\dot{x}_2 + k_2x_2 + m_1\ddot{x}_1 &= 0 \end{aligned}$$

with the initial conditions $x_1(0) = x_2(0) = 0$ and $\dot{x}_1(0) = \dot{x}_2(0) = v_0$. Using the relations $\mathrm{L}\{x(t)\} = X(s)$, $\mathrm{L}\{\dot{x}(t)\} = sX(s) - x(0)$, and $\mathrm{L}\{\ddot{x}(t)\} = s^2X(s) - sx(0) - \dot{x}(0)$, the Laplace transform of the system equations is

$$\begin{aligned} m_1(s^2X_1 - v_0) + c_1sX_1 + k_1X_1 - c_1sX_2 - k_1X_2 &= 0 \\ m_2(s^2X_2 - v_0) + c_2sX_2 + k_2X_2 + m_1(s^2X_1 - v_0) &= 0 \end{aligned}$$

or, in a compact matrix form,

$$\mathbf{AX} = \mathbf{B} \tag{4.1}$$

where $\mathbf{A} = \begin{pmatrix} m_1 s^2 + c_1 s + k_1 & -c_1 s - k_1 \\ m_1 s^2 & m_2 s^2 + c_2 s + k_2 \end{pmatrix}$, $\mathbf{X} = \{X_1 \quad X_2\}^T$, and $\mathbf{B} = \{m_1 v_0 \quad (m_1 + m_2) v_0\}^T$. Equation (4.1) is a set of two linear algebraic equations in $\mathbf{X}$ and thus can be solved using the matrix method. The solution set is

$$\mathbf{X} = \mathbf{A}^{-1}\mathbf{B} = \frac{\text{adj}\,\mathbf{A}}{\det \mathbf{A}}\,\mathbf{B}$$

or

$$\begin{pmatrix} X_1 \\ X_2 \end{pmatrix} = \frac{1}{\det \mathbf{A}} \begin{pmatrix} m_2 s^2 + c_2 s + k_2 & c_1 s + k_1 \\ -m_1 s^2 & m_1 s^2 + c_1 s + k_1 \end{pmatrix} \begin{pmatrix} m_1 \\ m_1 + m_2 \end{pmatrix} v_0$$

where

$$\begin{aligned} \det \mathbf{A} = {} & m_1 m_2 s^4 + (m_1 c_1 + m_1 c_2 + m_2 c_1) s^3 + (m_1 k_1 + m_1 k_2 + m_2 k_1 + c_1 c_2) s^2 \\ & + (k_1 c_2 + k_2 c_1) s + k_1 k_2 \end{aligned}$$

Therefore, the displacements of the two rigid masses, X_1 and X_2, in the complex s domain are, respectively,

$$\begin{aligned} X_1(s) &= v_0 \frac{m_1 m_2 s^2 + (m_1 c_1 + m_1 c_2 + m_2 c_1) s + (m_1 k_1 + m_1 k_2 + m_2 k_1)}{\det \mathbf{A}} \\ X_2(s) &= v_0 \frac{m_1 m_2 s^2 + (m_1 c_1 + m_2 c_1) s + (m_1 k_1 + m_2 k_1)}{\det \mathbf{A}} \end{aligned}$$

The displacement ratio, X_1/X_2, sometimes termed motion transmissibility, is then

$$\frac{X_1}{X_2} = \frac{m_1 m_2 s^2 + (m_1 c_1 + m_1 c_2 + m_2 c_1) s + (m_1 k_1 + m_1 k_2 + m_2 k_1)}{m_1 m_2 s^2 + (m_1 c_1 + m_2 c_1) s + (m_1 k_1 + m_2 k_1)}$$

The complex accelerations of the masses in the s domain are calculated by multiplying each complex displacement by s^2 and adding $-v_0$ to it, resulting

$$
\begin{aligned}
A_1(s) &= s^2 X_1(s) - v_0 \\
&= s^2 v_0 \frac{m_1 m_2 s^2 + (m_1 c_1 + m_1 c_2 + m_2 c_1)s + (m_1 k_1 + m_1 k_2 + m_2 k_1)}{\det \mathbf{A}} - v_0 \\
&= v_0 \frac{-c_1 c_2 s^2 - (k_1 c_2 + k_2 c_1)s - k_1 k_2}{\det \mathbf{A}} \\
A_2(s) &= s^2 X_2(s) - v_0 \\
&= s^2 v_0 \frac{m_1 m_2 s^2 + (m_1 c_1 + m_2 c_1)s + (m_1 k_1 + m_2 k_1)}{\det \mathbf{A}} - v_0 \\
&= v_0 \frac{-m_1 c_2 s^3 - m_1 k_2 s^2 - (k_1 c_2 + k_2 c_1)s - k_1 k_2}{\det \mathbf{A}}
\end{aligned}
$$

The acceleration ratio, denoted as $F(s)$, is thus

$$
F(s) = \frac{A_1(s)}{A_2(s)} = \frac{c_1 c_2 s^2 + (k_1 c_2 + k_2 c_1)s + k_1 k_2}{m_1 c_2 s^3 + m_1 k_2 s^2 + (k_1 c_2 + k_2 c_1)s + k_1 k_2}
$$

In the frequency domain, the acceleration ratio as a function of ω, the transmissibility function, is obtained by substituting s with $j\omega$, leading to

$$
F(j\omega) = \frac{-c_1 c_2 \omega^2 + (k_1 c_2 + k_2 c_1)j\omega + k_1 k_2}{-m_1 c_2 j\omega^3 - m_1 k_2 \omega^2 + (k_1 c_2 + k_2 c_1)j\omega + k_1 k_2}
$$

The complex expression for $F(j\omega)$ can be written in the form $|F(j\omega)|e^{j\angle F(j\omega)}$, and it can be shown that the expressions for both the magnitude, $|F(j\omega)|$, and the phase, $\angle F(j\omega)$, contain the system parameters m_1, k_1, k_2, c_1, and c_2.

The same analytical procedure can be applied to a translational system with more than two degrees of freedom, such as the one shown in Figure 4.2. The system equations of motion for this three-degree-of-freedom system are

$$
\begin{aligned}
m_0 \ddot{x}_0 + c_0(\dot{x}_0 - \dot{x}_1) + k_0(x_0 - x_1) &= 0 \\
m_1 \ddot{x}_1 + c_1(\dot{x}_1 - \dot{x}_2) + k_1(x_1 - x_2) + m_0 \ddot{x}_0 &= 0 \\
m_2 \ddot{x}_2 + c_2 \dot{x}_2 + k_2 x_2 + m_0 \ddot{x}_0 + m_1 \ddot{x}_1 &= 0
\end{aligned}
$$

with the initial conditions $x_0(0) = x_1(0) = x_2(0) = 0$ and $\dot{x}_0(0) = \dot{x}_1(0) = \dot{x}_2(0) = v_0$, and the complex acceleration ratio A_1/A_2, or transmissibility function, in ω is given also in Figure 4.2 with its complicated derivation given in Appendix A. It is apparent that the transmissibility is dependent not only on the mechanical properties of the elastic elements between the two points of the system across which the transmissibility is calculated, but also on that of many other parameters of the system.

4.2 Transmissibility of the Knee Joint

The human body is extremely complex even when considered to be a simplified mechanical system. However, in situations where the body experiences vertical forces of low amplitudes with frequency content below 100 Hertz, one could apply the lumped-parameter method to model the skeletal system by approximating all the long bones as being rigid masses and all the relevant soft tissues and cancellous subchondral bones as elastic elements contributing to the restoring and damping forces (von Gierke and Goldman, 1976). Thus, when a person walks, especially when barefooted, each leg along with the rest of the body is subjected to vertical velocity shocks that initiate transient vibration waves. The transmissibility function across the knee can be experimentally obtained by forming the ratio of digital Fourier transforms of two sets of acceleration data acquired from two transducers strapped across the knee.

As discussed earlier, such a transmissibility function will depend on the properties of the bone masses, subchondral bone, articular cartilage and other connective

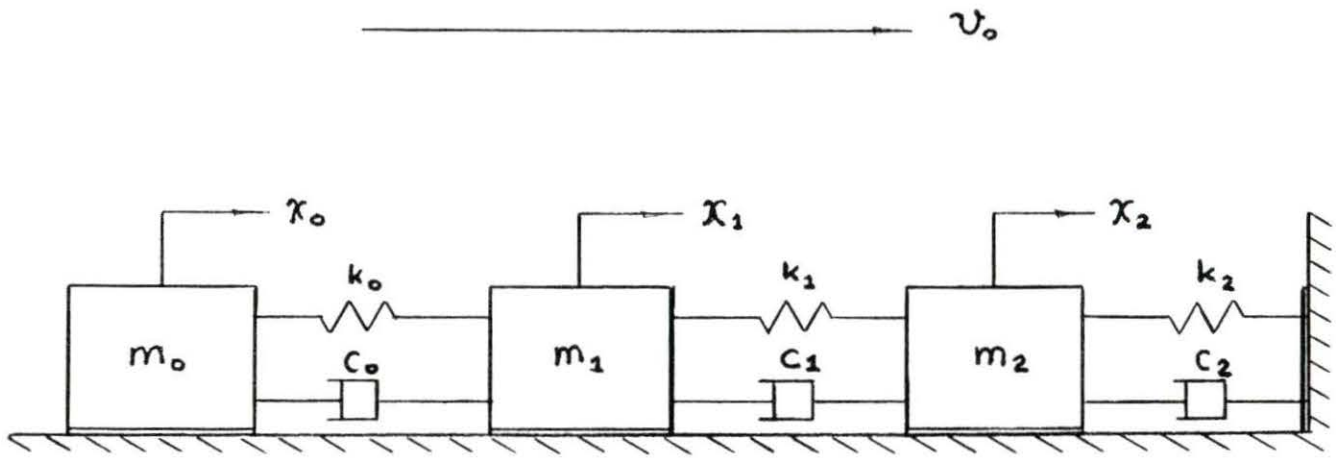

$$F(j\omega) = \{m_0c_1c_2\omega^4 - (m_0k_1c_2 + m_0k_2c_1 + c_0c_1c_2)j\omega^3 - (m_1k_1k_2 + k_0c_1c_2 + k_1c_0c_2 + k_2c_0c_1)\omega^2 + (k_0k_1c_2 + k_0k_2c_1 + k_1k_2c_0)j\omega + k_0k_1k_2\} /$$
$$\{m_0m_1c_2j\omega^5 + m_0m_1k_2 + m_0c_1c_2 + m_1c_0c_2)\omega^4 - (m_0k_1c_2 + m_0k_2c_0 + m_0k_2c_1 + m_0c_0c_2 + m_1k_0c_2 + m_1k_2c_0 + c_0c_1c_2)j\omega^3$$
$$-(m_0k_0k_2 + m_0k_0c_2 + m_0k_1k_2 + m_1k_0k_2 + k_0c_1c_2 + k_1c_0c_2 + k_2c_0c_1)\omega^2 + (k_0k_1c_2 + k_0k_2c_1 + k_1k_2c_0)j\omega + k_0k_1k_2\}$$

Figure 4.2: A system with three degrees of freedom in velocity shock and the derived transmissibility function from m_1 to m_2

tissues, the initial conditions of the system, and possibly the presence of muscle contraction. In addition, the rotational movement of the leg is of concern. At the moment of the heel strike, the leg is at an angle a little less than 90 degrees to the floor surface while the other leg continues to sustain a portion of the body weight. This situation definitely contributes to the determination of the transmissibility of the knee. Only when all of these extraneous factors are held constant, will one be able to characterize any changes in mechanical properties of the subchondral bone and the articular cartilage over a period of time.

5 METHOD

5.1 Instrumentation

Figure 5.1 displays a photographic view of the knee with two accelerometers strapped and Figure 5.2 shows the rest of the experimental set-up. A block diagram illustrating various components is given in Figure 5.3. The instrumentation consisted of four major parts: sensing, analog filtering, data acquisition, and analysis and display.

Two small mass accelerometers (Type 303A02, PCB Piezotronics, 3425 Walden Avenue, Depew, New York 14043) and a four-channel multi-gain amplifier unit (Model 482A04, PCB Piezotronics, 3425 Walden Avenue, Depew, New York 14043) constituted the sensing system. Each of the two accelerometers weighed 2.3 grams, had a resolution of $0.01g$ ($1g = 9.8m/s^2$) and a flat frequency response up to 1000 Hertz, and produced 10 millivolt output for every g. A 20-foot lightweight and soft coaxial cable, long enough to permit the subject to complete eight to ten walking cycles without hindrance, connected the transducer and the amplifier.

During the pilot test period of the project, the two transducers were found to generate large DC drift. Because of the miniature size, quartz material inside the transducer was so tightly packed that a small change in ambient temperature,

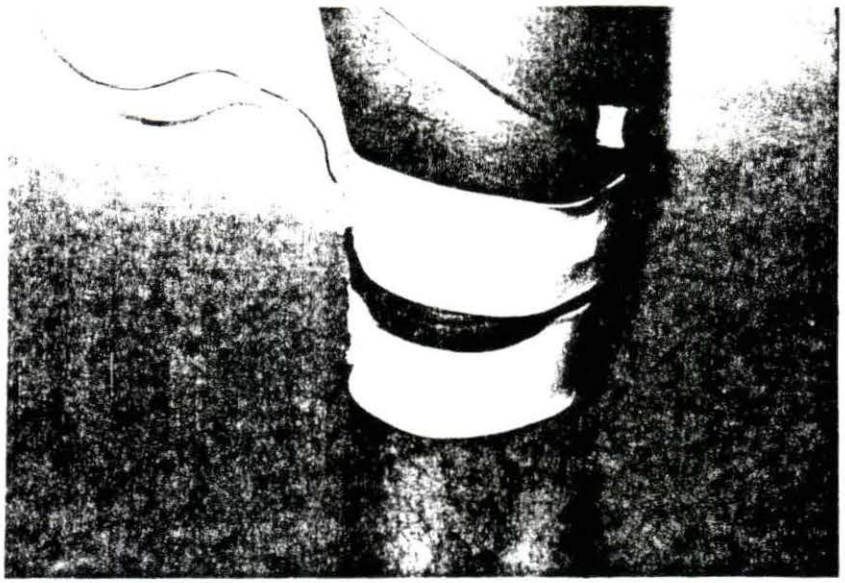

Figure 5.1: A photograph of a knee with two accelerometers strapped

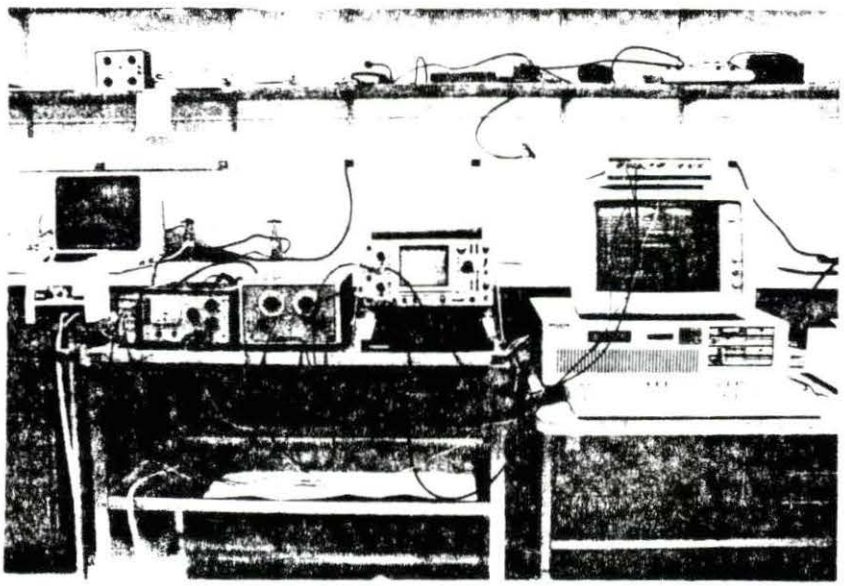

Figure 5.2: A photograph showing the power unit, prefilter, oscilloscope, A/D board, and IBM PC-AT connected

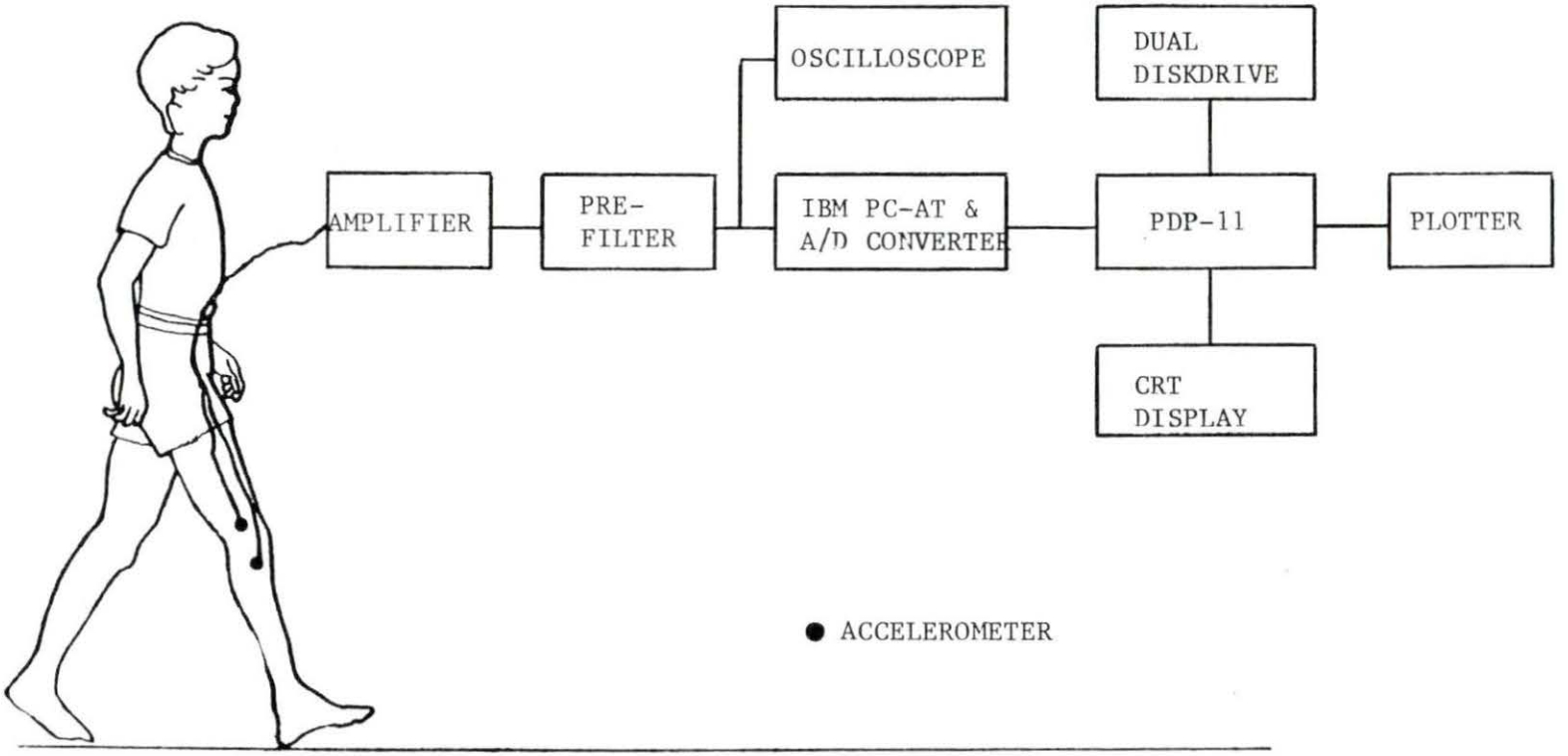

Figure 5.3: Block diagram of the experimental set-up

from room temperature to body temperature for example, caused a noticeable DC shift at the output port of the sensing unit. The drift settled down after five to ten minutes and, as a consequence, the subject had to wear the two accelerometers and the elastic bands for ten minutes before reliable recordings could be conducted. This caused extreme discomfort to the subject. To minimize the DC drift, the transducers were first kept under a surgical heat pad with its temperature set at a level a little lower than the body temperature before being strapped onto the knee. The unity-gain setting on the amplifier unit was also used to further reduce the thermal-coupled noise.

Before being digitally converted, transduced voltage signals had to pass through a two-channel Krohn-Hite electronic analog filter. This filter served as a low-pass antialiasing prefilter so as to guarantee the highest frequency of the signals before the conversion to be less than one half of the sampling frequency, as required by the Nyquist sampling theory (Jackson, 1986). The selected cut-off frequency of the prefilter was 75 Hertz as the impulsive loading forces at heel strike have no frequency components higher than 75 Hertz and thus could only excite the vibration modes of the tibia-knee-femur system between DC and 75 Hertz (Folman *et al.*, 1986; Roberts *et al.*, 1986).

Data acquisition was performed using a Keithley Data Acquisition system with its supporting software (SOFT500). Two channels sampled analog voltage signals simultaneously. Digitally converted signals then were stored in an IBM Personal Computer-AT microcomputer which also functioned to control the data acquisition board. Also shown in Figure 5.3 is a two-channel Tektronix analog oscilloscope,

between the prefilter and the data acquisition board, used for on-line observations of the registered signals.

The initially acquired data were found to be contaminated not only with thermal-coupled DC drift but also with noise thought to result from two long electrical leads between the transducers and the amplifier unit and other sources due to imperfection of the instrumentation and/or from behavioral changes of the subject. With the assumption that the noise was approximately random, it was attempted to design a triggering switch which could be attached to the foot of interest to allow for data averaging in the time domain. The first of the two initial designs was a pressure switch taped underneath the heel. It was composed of a thin layer of electrostatic foam sandwiched by two copper sheets. The second was a long-lever microswitch attached on the back side of the heel with double-sided adhesive tape. Each switch would be activated upon heel strike. However, because of some damping effect on the foot and long electrical delay introduced by the two switches, the final form of the switch to trigger the acquisition process was simply a microswitch held by an assistant (see Appendix B for descriptions of the switch and of the data acquisition program). This switch merely served to trigger the data acquisition process after the subject had completed several walking cycles to establish normal gait. Other measures of noise reduction were using coaxial cables for all the electrical connections, training the subject to walk nearly consistent steps, and data averaging in the frequency domain.

A DEC PDP-11 minicomputer with a Houston Instrument plotter was used to analyze the acquired acceleration data and plot the results. The choice of the

PDP-11 for data processing instead of the IBM PC-AT was due to

1. its high processing speed; it would take much less time to process large arrays of data, and

2. the accessibility of a well-supported high-quality plotter connected to the PDP-11.

5.2 Procedures

The experimental procedure was divided into two phases. The first phase, data acquisition, consisted of collection of acceleration data of vibrating bones using the microcomputer, and data transfer and storage with the minicomputer. The second phase involved data processing in which the stored data were mathematically manipulated to formulate the transmissibility function of the knee.

5.2.1 Data acquisition

The data acquisition process was controlled by the IBM PC-AT. Two commercially available 1.5-inch-wide elastic bands with Velcro pads sewn at the ends were used to strap the accelerometers onto the tibial lateral condyle and the femoral medial condyle (see Figure 5.1). The choice of a different site on the tibia, that is, the lateral tibial condyle instead of the tibial tuberosity, was to make sure that the two accelerometers would not only be in alignment with the longitudinal axis of the subject's stretched leg but also experience the same damping effects due to the underlying soft tissue.

The subject was asked to walk naturally with bare feet over a vinyl-on-concrete floor followed by an assistant carrying the two electrical accelerometer leads and the triggering switch. The triggering switch was activated by the assistant to start data acquisition after the subject had walked a few steps to establish his or her normal gait.

The sampling frequency was 500 Hertz per channel (a sampling interval of 2 milliseconds), which allows for frequency resolution up to 250 Hertz, much higher than the anticipated maximum of 75 Hertz. The sampling frequency was also high enough to provide a sufficient number of data points (128 points for the transient period) for the subsequent digital processing. The data acquisition phase lasted more than two seconds to allow for the recording of the time history of two complete walking cycles.

The data records were later transferred to the PDP-11 minicomputer using the communications protocol KERMIT and stored on a floppy disk.

5.2.2 Data processing

The data processing was done digitally on the PDP-11 minicomputer. Both signals recorded from below and above the knee underwent an identical preprocessing treatment before the calculation of the transmissibility function (see Appendix C for program listings).

Each time record was first filtered by a third-order digital Butterworth low-pass filter with a cut-off frequency of 75 Hertz to rid the signal of high frequency noise that may have added to the signal after the antialiasing filter. Initially, it was

also intended to subject each record to a high-pass filter to eliminate unwanted DC drift due to any imperfection of the instrumentation. The idea was later dropped because of high attenuation to the low frequency components of the signal. To avoid tedious algebra in design of the digital Butterworth filters, a FORTRAN program was implemented to aid in their design. The program description and listing are detailed in Appendix D.

A FORTRAN program was written to perform the rest of the data analysis. It started with locating the second acceleration peak of the filtered signal and multiplying it by a unit square window function so that the resulting series was the time history of only one transient period. The linear regression of the signal on time was subtracted from it to compensate for DC drift. The record then was subjected to Hanning windowing to minimize the effect of discontinuities at the two ends of the time series prior to Fourier transformation (Oppenheim and Schafer, 1975; Ramsey, 1975; Taylor and Smith, 1976).

The discrete Fourier transformation was performed using an FFT algorithm. To make sure it would work properly, the FFT routine was tested with several known functions. A zero-padding technique was also used to increase spectral resolution. Descriptions and sample plots of the FFT and the zero-padding method can be found in Appendix E.

The transmissibility function $F(j\omega)$, defined as the ratio of the discrete Fourier transform of the acceleration of the tibia to that of the femur, was calculated. The magnitude and phase of the transmissibility function were plotted against frequency.

Also calculated was the crosscorrelation function of the two accelerations ob-

tained across the knee which would provide information on how, with the presence of the resilient elements between the two long bones, the motion of the femur would follow that of the tibia during velocity shock. By definition, the crosscorrelation function of two continuous time functions $x(t)$ and $y(t)$ is given by $R_{xy}(\tau)$, where

$$R_{xy}(\tau) = \lim_{T\to\infty} \frac{1}{T} \int_T x(t)y(t-\tau)\,dt$$

which measures how closely the two time functions are related to each other when one is shifted in time by τ seconds. Since digital computers only work on discrete functions, and since it is impossible to collect data over an infinite time period T, an approximation is given as

$$R_{xy}(n\Delta\tau) = \frac{1}{N\Delta t} \sum_{k=0}^{N-1} x(k\Delta t)y(k\Delta t - n\Delta\tau)$$

where N is the number of sampled data points, n the running variable, Δt the sampling interval, and $\Delta\tau$ normally chosen to be equal to Δt. This approximation is good only when $n\Delta\tau$ is small compared to $N\Delta t$, the total length of the time record (Russell, 1978). Typically used is the normalized crosscorrelation function, sometimes called the correlation coefficient function, given as

$$r_{xy}(n\Delta\tau) = \frac{R_{xy}(n\Delta\tau)}{\sqrt{R_{xx}(0)R_{yy}(0)}}$$

where $R_{xx}(0)$ and $R_{yy}(0)$ are, respectively, the autocorrelation functions of $x(t)$ and $y(t)$ evaluated at $n = 0$. For example,

$$R_{xx}(0) = \frac{1}{N\Delta t} \sum_{k=0}^{N-1} x(k\Delta t)x(k\Delta t)$$

The function $r_{xy}(n\Delta\tau)$ is bounded between plus and minus one.

Finally, the percentage of the DFT magnitude to the total spectrum was calculated and plotted to show how the spectral energy was distributed.

5.3 Reproducibility

One of the difficulties in applying engineering methods to biological studies lies in the degree of reproducibility of an experimental design, as a biological system constantly undergoes both physical and behavioral changes. In the design process of such an experiment involving biological data acquisition and analysis, care must be given to assure the reproducibility of the experiment. Toward this end, a statistical analysis was conducted to determine reproducibility of the undertaken experiment. The analysis was to calculate the correlation coefficient between two sets of data obtained at two different experimental sessions to determine the degree of their similarity or the strength of their relationship (Cox, 1987).

Five sets of acceleration data were collected from the same subject on five different experimental sessions and the correlation coefficient between each pair of data sets was calculated using the Statistical Analysis System (SAS) on the Iowa State University Computation Center's NAS AS/9160 computer. The latter was performed at several different stages through the data analysis process to determine if the mathematical manipulation had any effect on the reproducibility.

6 RESULTS AND DISCUSSION

Figures 3.1 and 6.1 through 6.7 display a set of plots in different stages of the data analysis. The acceleration data were taken from the right leg of a male subject with no diagnosed knee disorder. A comparison between Figures 3.1 and 6.1 shows little effect of the low-pass filtering of the acquired data, suggesting that the instrumentation was immune to high frequency noise.

The peak acceleration transient of the tibia was around $6g$ with its subsequent reverberation greatly damped. This is consistent with other investigator's findings (Light and McLellan, 1977; Voloshin and Wosk, 1984). The facts that the onset peak of the femur is about $3.5g$, much less than that of the tibia, and that the apparent shift in time of the peak clearly indicate the presence of a "cushion" between the two long bones. The two accelerations reached their peaks less than 20 milliseconds after heel strike. Within this short period of time, muscle reaction was not likely to contribute to the attenuation of the peak forces. However, the presence of muscle tone might have played a role in absorbing some of the transmitted vibrational energy.

In the plots of the DFT magnitudes (Figure 6.4), the three major peaks on each curve are indications of three major vibration modes of the leg system, as the frequencies of maximum acceleration response are approximately equal to the

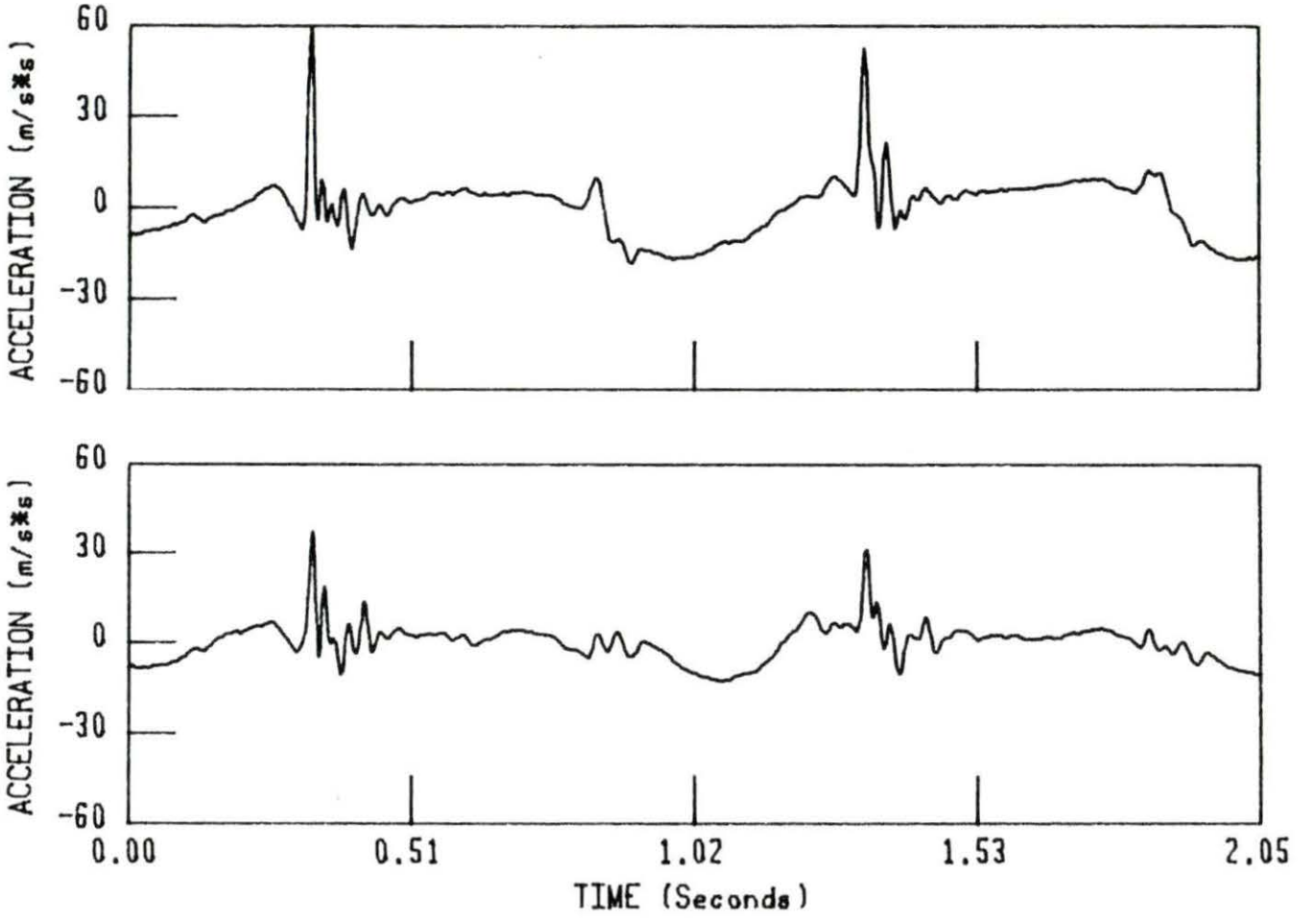

Figure 6.1: Acceleration plots after being low-pass (75 Hertz) filtered. Tibia–top plot; femur–bottom plot

resonant frequencies (Ewins, 1984; Jurist, 1970). The magnitude spectra extended over 60 Hertz. The spectrum of the femoral vibration has smaller values than that of the tibial vibration in general with the exceptions in two frequency ranges, one between 10 and 16 Hertz and another between 34 and 39 Hertz. If the leg were excited by a single vertical sinusoidal force of a frequency in any of the two ranges, the femur would vibrate with a larger displacement than the tibia. All of the above is in clear contrast with the results of Voloshin and Burger's (1982) study in which only two vibration modes were evident, the magnitude spectra only resided from DC to 25 Hertz, and the tibial spectrum had larger values than the femoral counterpart throughout the chosen frequency range. Some possible reasons for the discrepancies might be differing choices of the time span of the acceleration data from which the DFT was calculated, or band-pass filtering might have been performed on the registered data, giving the smooth-looking time history plots in their paper.

In the frequency range of DC to 14 Hertz in which the first vibration mode occurred, there was no phase difference between the vibrational motions of the two long bones, as evident in Figure 6.5, and the difference in magnitude was also minimal. This implies that, in this frequency range, the tibia and the femur were vibrating in phase and with essentially identical amplitudes so that the length of the spring element in between remained constant (von Gierke and Goldman, 1976; Rao, 1986). Around 25 Hertz, the phase difference again became zero but the two magnitudes differed by more than 50 percent, showing that, although the motions of the two masses were in phase, the displacement of the femur was much

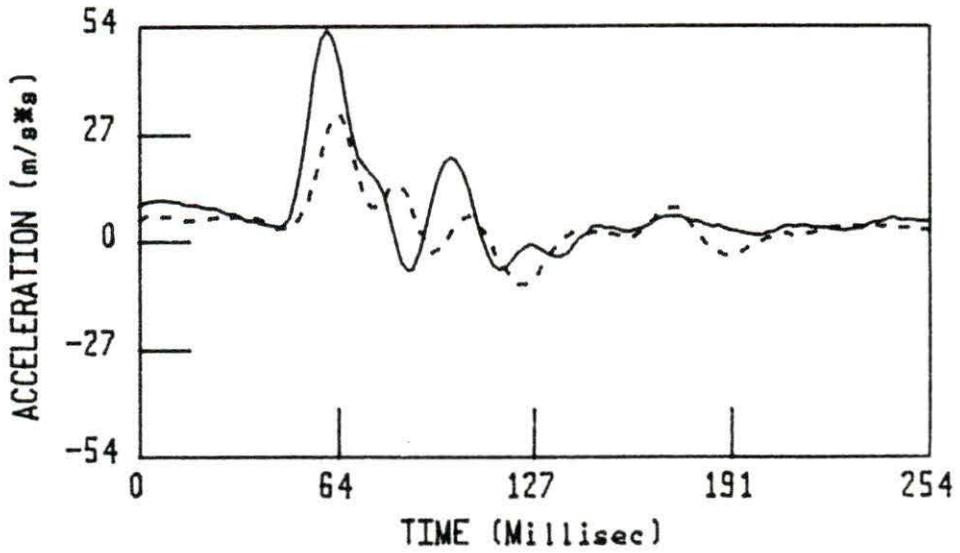

Figure 6.2: Square-windowed signals of the transient period. Tibia—solid line; femur—dashed line

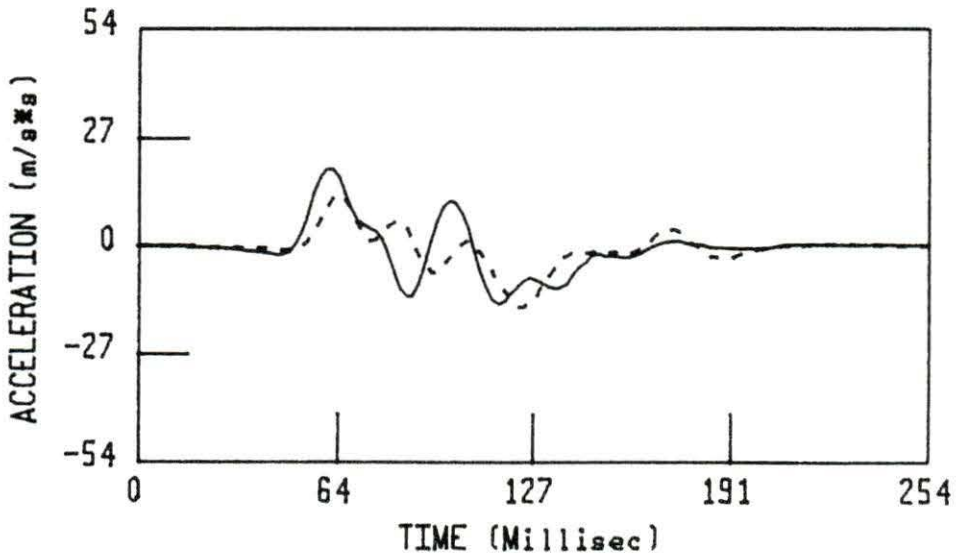

Figure 6.3: Signals after preprocessing. Tibia—solid line; femur—dashed line

smaller than that of the tibia due mainly to the damping effect of the resilient element in between. This difference should provide information on how effective the resilient elements, namely the subchondral bones and the articular cartilage, are in absorbing vibrational energy. Therefore, in relating this factor to the progression of an osteoarthritic condition of a knee joint, one would expect to observe in Figure 6.4 a decrease in, or a shift of, the area bounded by the two curves between 18 and 30 Hertz over a period of time.

In any other frequency ranges, the two bones vibrated out of phase. The characteristics of their motions were dependent of all the system parameters and, therefore, too complicated for one to extract any useful information about the mechanical properties of the subchondral bones and the articular cartilage of the knee joint.

The transmissibility function plots in Figures 6.6 and 6.7 reinforce what is evident in the DFT plots. In the two frequency ranges where the phase is zero, the magnitude of the transmissibility function is either unity or minimum.

No matter how different the two DFT magnitude plots in Figure 6.4 look from each other, 50 percent of the total spectral energy of either resides between DC and 28 Hertz and 90 percent lies below 60 Hertz, as shown in Figure 6.8. This serves to further validate the assumption that the lumped-parameter method could be applied to the leg system.

The crosscorrelation function between the tibial and femoral accelerations plotted in Figure 6.9 has a maximum value close to unity at $\tau = 4$ milliseconds. It shows that, on the average, the acceleration transient of the femur was following that of

the tibia but lagging behind for four milliseconds. Intuitively, this time lag resulted from the elastic properties of the knee joint. Therefore, a change in where this maximum occurs over a period of time might indicate a change in the properties of the subchondral bones and the articular cartilage. To accurately detect any time shift calls for higher sampling frequency than 500 Hertz, which the Keithley Data Acquisition system in use does not permit.

Table 6.1 lists the correlation coefficients between five tibial acceleration records taken at five different experimental sessions. $\bar{r}_t$ is the sample mean of the ten coefficients and its value is close to unity, an indication of good reproducibility of the experimental design.

$\bar{r}_f$ in Table 6.2 is the sample mean of the ten coefficients between five femoral acceleration records and its value is also close to unity, though not as close as that of $\bar{r}_t$.

The correlation coefficients similarly calculated of five DFT magnitudes are listed in Tables 6.3 and 6.4. As can be seen, the correlation of the DFTs of the tibial data was not as good as that in the time domain, whereas an increase in the degree of correlation of the DFTs of the femoral accelerations was evident. No explanation was found for the inconsistency.

$\bar{r}_{FT}$ in Table 6.5 is the sample mean of the ten correlation coefficients between magnitudes of five transmissibility functions resulting from the five acceleration records. The value was found to be 0.73012, quite small compared to those of $\bar{r}_t$, $\bar{r}_f$, $\bar{r}_T$, and $\bar{r}_F$. The result is contrary to the initial belief that the transmissibility function would be more reproducible because the division of $A_f(j\omega)$, the Fourier

transform of the femoral acceleration, by $A_t(j\omega)$, the Fourier transform of the tibial acceleration, would cancel any noise common to the two accelerometers strapped across the knee joint. Though their correlation coefficients are not close to unity, the plots of the magnitudes of the five transmissibility functions in Figure 6.10 all reveal the same distinctive shape.

The best correlation was found between the five crosscorrelation functions. The sample mean, $\bar{r}_c$, was found to have a value of 0.97272, as shown in Table 6.6. This, along with the information given above, shows that the major portion of the contaminating noise which degraded the correlation of the two acceleration signals recorded from across the knee was common to the two transducers.

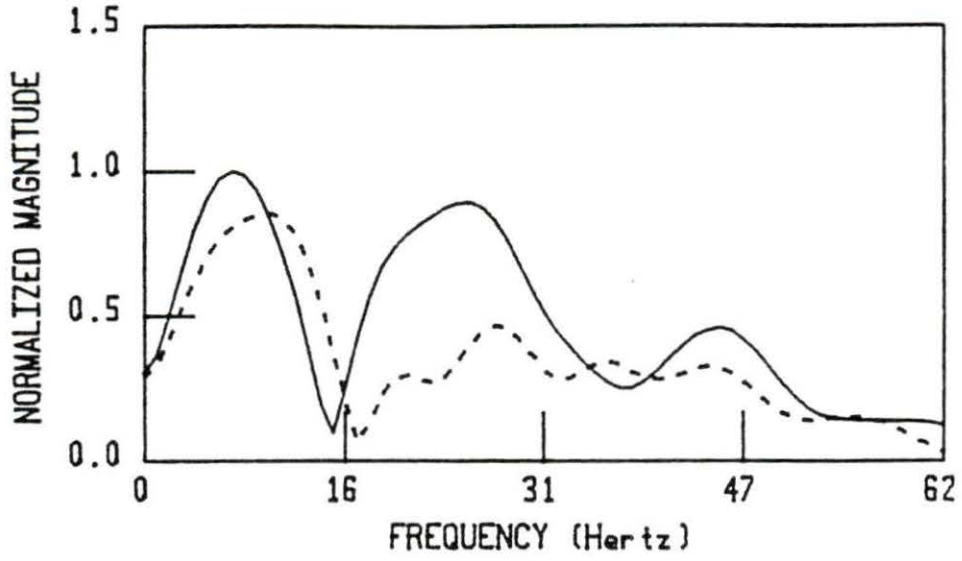

Figure 6.4: DFT magnitude plots. Tibia—solid line; femur— dashed line

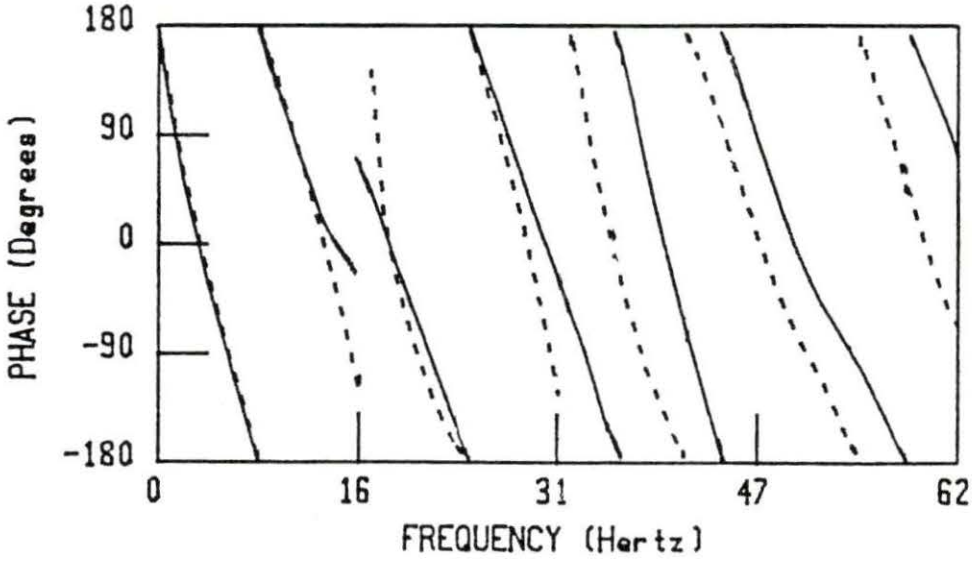

Figure 6.5: DFT phase plots. Tibia—solid line; femur—dashed line

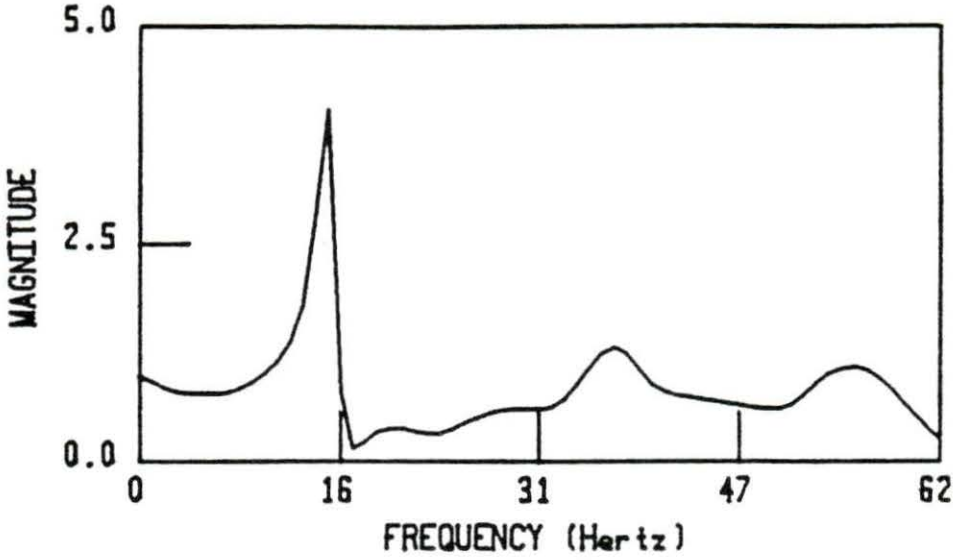

Figure 6.6: Magnitude of transmissibility function

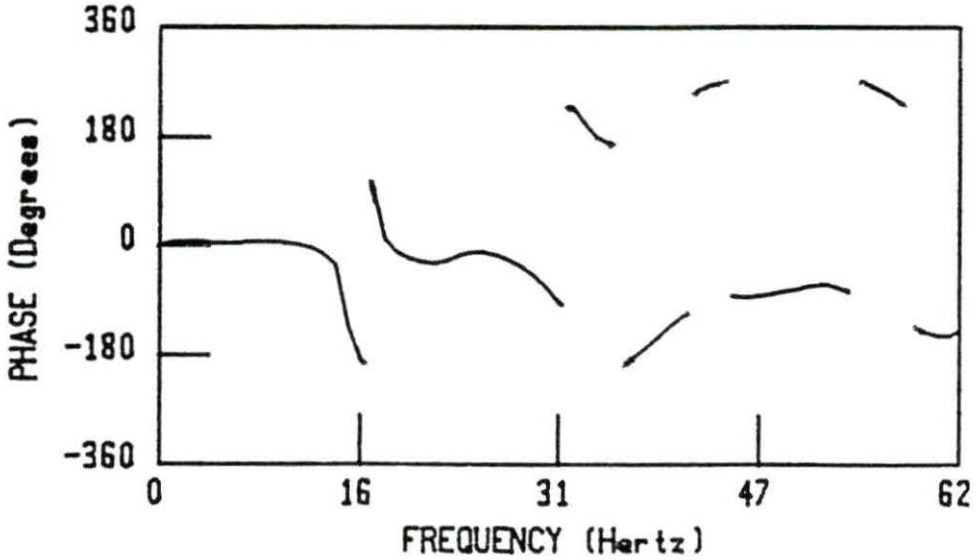

Figure 6.7: Phase of transmissibility function

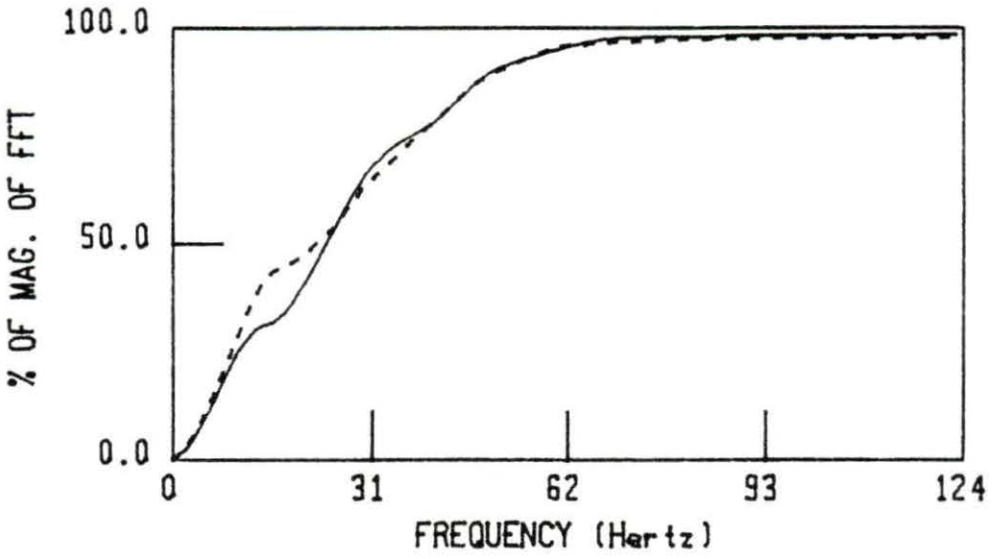

Figure 6.8: Percentage to the total magnitude spectrum as a function of frequency. Tibia—solid line; femur—dashed line

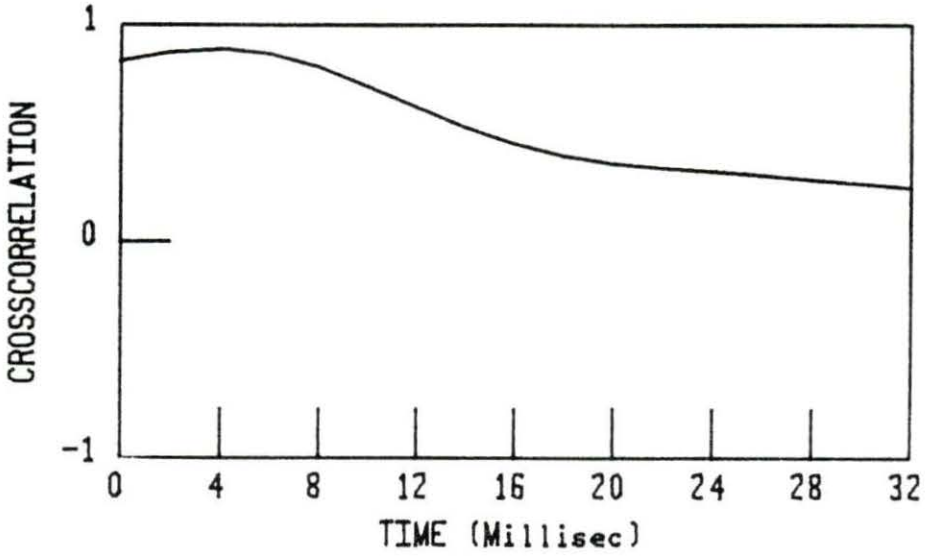

Figure 6.9: Crosscorrelation function of the two accelerations across the knee

Table 6.1: Correlation coefficients, r_t, between five tibial acceleration records taken at different times

	Record 1	Record 2	Record 3	Record 4	Record 5
Record 1	-	0.95	0.95	0.97	0.97
Record 2	-	-	0.98	0.95	0.97
Record 3	-	-	-	0.95	0.97
Record 4	-	-	-	-	0.98
Record 5	-	-	-	-	-
$\bar{r}_t = 0.96$					

Table 6.2: Correlation coefficients, r_f, between five femoral acceleration records taken at different times

	Record 1	Record 2	Record 3	Record 4	Record 5
Record 1	-	0.87	0.90	0.91	0.87
Record 2	-	-	0.92	0.93	0.94
Record 3	-	-	-	0.93	0.95
Record 4	-	-	-	-	0.98
Record 5	-	-	-	-	-
$\bar{r}_f = 0.92$					

Table 6.3: Correlation coefficients, r_T, between magnitudes of five DFTs of the tibial acceleration records

	Record 1	Record 2	Record 3	Record 4	Record 5
Record 1	-	0.92	0.86	0.90	0.90
Record 2	-	-	0.95	0.93	0.93
Record 3	-	-	-	0.83	0.90
Record 4	-	-	-	-	0.88
Record 5	-	-	-	-	-
$\bar{r}_T = 0.90$					

Table 6.4: Correlation coefficients, r_F, between magnitudes of five DFTs of the femoral acceleration records

	Record 1	Record 2	Record 3	Record 4	Record 5
Record 1	-	0.90	0.92	0.95	0.95
Record 2	-	-	0.90	0.95	0.97
Record 3	-	-	-	0.87	0.94
Record 4	-	-	-	-	0.98
Record 5	-	-	-	-	-
$\bar{r}_F = 0.93$					

Table 6.5: Correlation coefficients, r_{TF}, between magnitudes of five transmissibility functions

	Record 1	Record 2	Record 3	Record 4	Record 5
Record 1	-	0.77	0.58	0.79	0.85
Record 2	-	-	0.67	0.78	0.90
Record 3	-	-	-	0.54	0.63
Record 4	-	-	-	-	0.79
Record 5	-	-	-	-	-
$\bar{r}_{FT} = 0.73$					

Table 6.6: Correlation coefficients, r_c, between five crosscorrelation functions of the five sets of the acceleration records

	Record 1	Record 2	Record 3	Record 4	Record 5
Record 1	-	0.97	0.94	0.96	0.94
Record 2	-	-	0.98	0.99	0.99
Record 3	-	-	-	0.99	0.99
Record 4	-	-	-	-	0.99
Record 5	-	-	-	-	-
$\bar{r}_c = 0.97$					

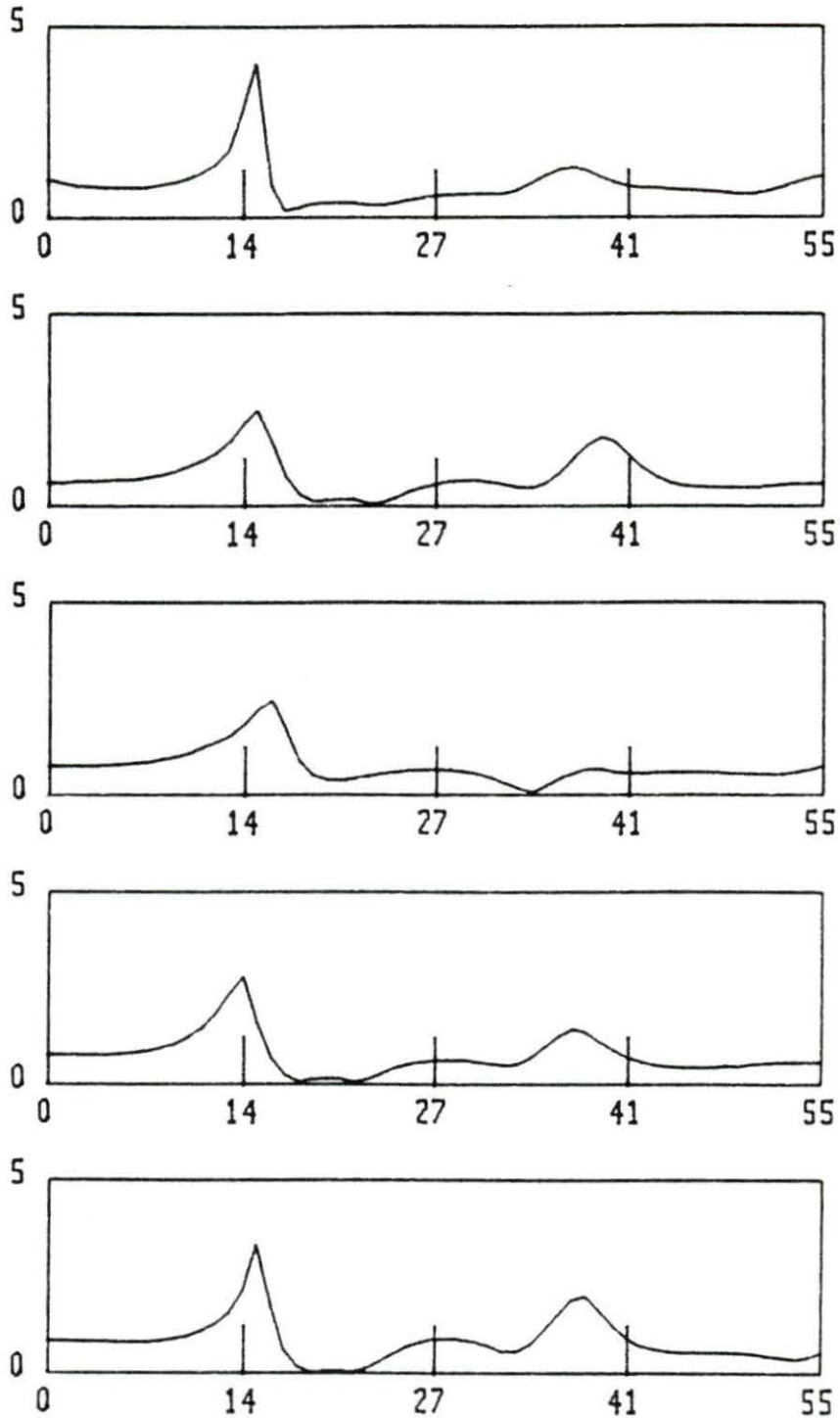

Figure 6.10: Magnitudes of transmissibility functions of five sets of vibration signals. Vertical axes–magnitudes; horizontal axes–frequency

7 SUMMARY AND CONCLUSIONS

The results of this study indicate a potential value of the digital accelerometric technique in *in vivo* evaluation of the osteoarthritic condition of the knee joint. With the understanding that the degenerative joint disease was a pathological process of not only disintegration of articular cartilage but also sclerosis of subchondral bones, with the latter believed to facilitate the former, the study demonstrated the following:

- Heel strikes during normal walking generated vibrational transients of the tibia, the femur, and other skeletal components. The power spectra of the tibial and femoral acceleration transients resided mainly in a frequency range from DC to 60 Hertz.

- In the course of heel strike, the human skeletal system could be modeled as a multi-degree-of-freedom vibratory system in velocity shock with the long bones such as the tibia and the femur lumped as rigid masses and the cancellous subchondral bones and various soft tissues such as the heel pad and articular cartilage as resilient elements.

- The transmissibility, defined as the ratio of $A_f(j\omega)$ and $A_t(j\omega)$, the Fourier transforms of the tibial and femoral transient accelerations, respectively, was

a function of the properties not only of the resilient elements between the tibia and the femur but also of other system elements such as bone masses. Thus, the characteristics of a transmissibility function may be different from subject to subject regardless of the pathological condition of his or her knee joint.

- The transients could be transduced to analog voltage signals by small mass accelerometers and digitized by an A/D converter. The digital records then could be used for calculation of the transmissibility function and other analysis with a digital computer.

- For the particular subject in this study, the leg system was found to have three major vibration modes at approximately 8 Hertz, 27 Hertz, and 44 Hertz, respectively.

- In a frequency range between DC and 14 Hertz, the tibia and the femur vibrated as if the two long bones were one rigid mass.

- The magnitude of the transmissibility function in a frequency range in which the tibia and femur vibrated in phase but with a large difference in displacement and the crosscorrelation function of the tibial and femoral accelerations might serve to provide useful information on how the degenerative joint disease of a patient progresses.

- Except for the transmissibility function, the reproducibility of the acceleration signals, crosscorrelation function of the signals, and the digital Fourier transforms of the signals was above 90 percent.

Because the transmissibility in general varies from one knee joint to another due to difference in properties of the related elements, the use of this digital accelerometric technique may be restricted to areas where documenting the progress of the osteoarthritic disease of knee joints is necessary. Nevertheless, it holds high promise as an additional tool in routine clinical evaluation of the integrity of human knee joints as a result of its noninvasive nature and simple procedure. It involves no drugs and requires minimal amount of preparation. The instrumentation could also be developed based on a single-board microcomputer to insure portability and low cost. In sports medicine, rehabilitation programs, hospitals, clinics, and the work of therapists and athletic trainers, the technique may find a variety of applications. Before this technique can be put to use by clinicians, however, extensive further study is needed in the following areas.

- Design of accelerometers. The instability of the accelerometers in the low frequency range reduces the reproducibility of acceleration signals and thus complicates the digital data analysis. Research should be conducted to find small accelerometers with good low frequency response. In addition, the shape of the accelerometer should be resigned to have a wide flat surface against the skin so as to eliminate any discomfort to the subject as well as to improve the reproducibility.

- Effect of muscle contraction and joint movement on the transmissibility function. Studies should be conducted to determine the contributions of muscle contraction and joint movement to the attenuation of the incoming vibrational energy. If these factors are too difficult to quantify, it is essential to find a way

of holding them constant for every subject in different experimental sessions.

- Reproducibility. An optimal procedure to train the subject needs to be designed so that behavioral changes of the subject in walking can be minimized. Also, theoretical and experimental explanations should be found for the low reproducibility of the transmissibility function.

- Effect of a change in properties of subchondral bones and articular cartilage. A sufficient number of subjects with or without confirmed osteoarthritic knee disorders should be tested for a long period of time to identify statistically how major spectral and crosscorrelation features change over time as the disease progresses. These tests should preferably corroborated by X-ray examinations and blood tests to insure subjectivity.

- Portability of the instrumentation. Research should be done to make the instrument partible so that it will fit in a clinical setting. In addition, both hardware and software should be designed to be user-friendly and test procedure simple to minimize the effort during the massive testing of the technique.

8 BIBLIOGRAPHY

Bihari-Varga, M., T. Farkas, and T. Biro. 1984. Changes in the cartilage proteoglycans in relation to age and osteoarthrosis. *Acta Biologica Hungarica* 35:325–331.

Burfoot A. 1986. No bones about it. *Runner's World* 6:63–65.

Chu, M. L., I. A. Gradisar, M. R. Railey, and G. F. Bowling. 1976. An electroacoustical technique for the detection of knee joint noise. *Medical Research Engineering* 12(1):18–20.

Chu, M. L., I. A. Gradisar, and L. D. Zavodney. 1978. Possible clinical application of a noninvasive monitoring technique of cartilage damage in pathological knee joints. *Journal of Clinical Engineering* 3(1):19–27.

Cox, C. P. 1987. A handbook of introductory statistical methods. *John Wiley and Sons, New York.*

Dekel, S., and S. L. Weissman. 1978. Joint changes after overuse and peak overloading of rabbit knees in vivo. *Acta Orthopaedica Scandinavica* 49:519-528.

Dickinson, J. A., S. D. Cook, and T. M. Leinhardt. 1985. The measurement of shock waves following heel strike while running. *Journal of Biomechanics* 18(6):415–422.

Ewins, D. J. 1984. Modal testing: Theory and practice. *Research Studies Press, Letchworth, Hertfordshir, England.*

Folman, Y., J. Wosk, A. Voloshin, and S. Liberty. 1986. Cyclic impacts on heel strike: A possible biomechanical factor in the etiology of degenerative dis-

ease of the human locomotor system. *Archives of Orthopaedic and Traumatic Surgery* 104:363– 365.

Jackson, L. B. 1986. Digital filters and signal processing. *Kluwer Academic, Boston.*

Kunz, J. R. M., and A. J. Finkel. 1987. Disorders of the muscles, bones and joints. Pages 540–568. In *Family Medical Guide, Random House, New York*

Jurist, J. M. 1970. In vivo determination of the elastic response of bone I. Method of ulnar resonant frequency determination. *Physics in Medicine and Biology* 15(3):417–426.

Light, L. H., and G. McLellan. 1977. Skeletal transients associated with heel strike. *Journal of Physiology* 272:9–10p.

Light, L. H., G. E. McLellan, and L. Klenerman. 1980. Skeletal transients on heel strike in normal walking with different footwear. *Journal of Biomechanics* 13:427–480.

Little, K., and L. H. Pimm. 1958. Osteoarthritis of the hip. An electro-microscope study. *Journal of Bone and Joint Surgery* 40:123-131.

Maquet, P. 1980. The biomechanics of the knee and surgical possibilities of healing osteoarthritic knee joints. *Clinical Orthopaedics and Related Research* 146:102–110.

Marcinko, D. E., and M. D. Dollard. 1986. Physical and Mechanical Properties of Joints (The pathomechanics of articular cartilage degeneration). *Journal of Foot Surgery* 25(1):3–13.

Mollan, R. A. B., G. W. Kernohan, and P. H. Watters. 1983. Artefact encountered by the vibration detection system. *Journal of Biomechanics* 16(3):193–199.

Morris, J. R. W. 1973. Accelerometry– a technique for the measurement of human body movements. *Journal of Biomechanics* 6:729–736.

Nokes, L., J. A. Fairchough, W. J. Mintowt-Czyz, I. Mackie, and J. Williams. 1984. Vibration analysis of human tibia: The effect of soft tissue on the output from skin-mounted accelerometers. *Journal of Biomedical Engineering* 6:223–226.

Oppenheim, L. R., and R. W. Schafer. 1975. Digital signal processing. *Prentice-*

Hall, Englewood Cliffs, New Jersey.

Paul, I. L., M. B. Munro, P. J. Abernethy, S. R. Simon, E. L. Radin, and R. M. Rose. 1978. Musculo-skeletal shock absorption: Relative contribution of bone and soft tissues at various frequencies. *Journal of Biomechanics* 11:237-239.

Radin, E. L., and I. L. Paul. 1972. Role of mechanical factors in pathogenesis of primary osteoarthritis. *The Lancet* 3:519-521.

Radin, E. L., and I. L. Paul. 1970. Does cartilage compliance reduce skeletal impact loads? (The relative force-attenuating properties of articular cartilage, synovial fluid, periarticular soft tissues and bone.) *Arthritis and Rheumatism* 13(2):139–144.

Radin, E. L., M. G. Ehrlich, R. Charnack, and P. J. Abernathy. 1978. Effect of repetitive impulsive loading on the knee joints in rabbits. *Clinical Orthopaedics and Related Research* 131:288-293.

Ramsey, K. A. 1975. Effective measurements for structural dynamics testing. *Sound and Vibration* 11:24–31.

Rao, S. S. 1986. Mechanical Vibrations. *Addison-Wesley Publishing, Menlo Park, California.*

Roberts, S., B. Weightman, J. Urban, and D. Chappell. 1986. Mechanical and biochemical properties of human articular cartilage in osteoarthritic femoral heads and in autopsy specimens. *Journal of Bone and Joint Surgery* 68-B(2):278–288.

Ruoff, G. E. 1986. The pain of osteoarthritis. *The American Journal of Medicine* 80:Suppl. 3A.

Russell, S. F. 1978. Spectral analysis methods for noisy sampled-data systems. *Ph. D. dissertation. Iowa State University,* Ames, Iowa.

Saha, S., and R. S. Lakes. 1977. The effect of soft tissue on wave-propagation and vibration tests for determining the in vivo properties of bone. *Journal of Biomechanics* 10:393–410.

Simon, S. R., I. L. Paul, J. Mansour, M. Munro, P. J. Abernethy, and E. L. Radin. 1981. Peak dynamic force in human gait. *Journal of Biomechan-*

ics 14(12):817–822.

Simon, S. R., E. L. Radin, I. L. Paul, and R. M. Rose. 1972. The response of joints to impact loading–II in vivo behavior of subchondral bone. *Journal of Biomechanics* 5:267–272.

Sokoloff, L. 1963. Elasticity of articular cartilage: effect of ions and viscous solutions. *Science* 141:1055–1057.

Spence, A. P., and E. B. Mason. 1983. Human Anatomy and physiology. *Benjamin/Cummings Publishing, Menlo Park, California.*

Stanley, W. D., and G. R. Dougherty. 1984. Digital Signal Processing. *Reston Publishing, Reston, Virginia.*

Taylor, F., and S. L. Smith. 1976. Digital signal processing in FORTRAN. *Lexington Books, Lexington, Massachusetts.*

Voloshin, A. S., and C. P. Burger. 1982. Transmissibility function of the healthy human knee (in vivo study). Pages 225– 228. S. Saha, ed. Proceedings of the First Southern Biomedical Engineering Conference, Sherveport, LA, June 7-8, 1982. In *Biomedical Engineering I, Recent Developments*. Pergamon Press, Oxford, England.

Voloshin, A. S., and J. Wosk. 1984. Does body weight significantly contribute to joint degeneration? *Journal of Clinical Engineering* 9(2):153–158.

Voloshin, A. S., and J. Wosk. 1983. Shock absorption of meniscectomized and painful knees: a comparative in vivo study. *Journal of Biomedical Engineering* 5:157-161.

Voloshin, A. S., and J. Wosk. 1982. An in vivo study of low back pain and shock absorption in the human locomotor system. *Journal of Biomechanics* 15(1):21–27

Voloshin, A. S., J. Wosk, and M. Brull. 1981. Force wave transmission through the human locomotor system. *Journal of Biomechanical Engineering* 103:48–50.

von Gierke, H. E., and D. E. Goldman. 1976. Effects of shock and vibration on man. Pages 44-1—44-57. *In* C. M. Harris and C. E. Crede, ed. Shock and Vibration Handbook. *McGraw-Hill Book, New York.*

Wong, F. Y., S. Pal, and S. Saha. 1983. The assessment of in vivo bone condition in humans by impact response measurement. *Journal of Biomechanics* 16(10):849–856.

Wosk, J., and A. S. Voloshin. 1981. Wave attenuation in skeletons of young healthy persons. *Journal of Biomechanics* 14(4):261–267.

Ziegert, J. C., and Lewis, J. L. 1979. The effect of soft tissue on measurements of vibrational bone motion by skin-mounted accelerometers. *Journal of Biomechanical Engineering* 101:218–220.

9 ACKNOWLEDGMENTS

I wish to express my sincere appreciation to my major professors, Dr. William H. Brockman and Dr. Patrick E. Patterson, for giving me the opportunity to conduct this research, and for their guidance, support, and encouragement throughout the research. I would also like to thank Dr. Philip Cox for serving on my committee, and Drs. R. Grover Brown, David F. Cox, and Kenneth G. McConnell for their valuable comments and suggestions on the project. I would like to acknowledge the much appreciated financial support I have received from Dr. Patrick E. Patterson and from the Biomedical Engineering Program, without which my education at Iowa State University would have been impossible.

Finally, I would like to extend my thanks to my parents at home for their extraordinary patience during the whole period of my higher education pursuit.

This project was approved by the University Committee on the Use of Human Subjects in Research.

10 APPENDIX A: DERIVATION OF THE TRANSMISSIBILITY FUNCTION OF A THREE-DEGREE-OF-FREEDOM SYSTEM

The system equations of the motion of the three-degree-of-freedom vibratory system in velocity shock, shown in Figure 4.2, are

$$\begin{aligned} m_0\ddot{x}_0 + c_0(\dot{x}_0 - \dot{x}_1) + k_0(x_0 - x_1) &= 0 \\ m_1\ddot{x}_1 + c_1(\dot{x}_1 - \dot{x}_2) + k_1(x_1 - x_2) + m_0\ddot{x}_0 &= 0 \\ m_2\ddot{x}_2 + c_2\dot{x}_2 + k_2x_2 + m_1\ddot{x}_1 + m_0\ddot{x}_0 &= 0 \end{aligned}$$

with the initial conditions $x_0(0) = x_1(0) = x_2(0) = 0$ and $\dot{x}_0(0) = \dot{x}_1(0) = \dot{x}_2(0) = v_0$. Using the relations $\mathrm{L}\{x(t)\} = X(s)$, $\mathrm{L}\{\dot{x}(t)\} = sX(s) - x(0)$, and $\mathrm{L}\{\ddot{x}(t)\} = s^2X(s) - sx(0) - \dot{x}(0)$, and taking the Laplace transform of the system equations lead to

$$\begin{aligned} m_0(s^2X_0 - v_0) + c_0s(X_0 - X_1) + k_0(X_0 - X_1) &= 0 \\ m_1(s^2X_1 - v_0) + c_1s(X_1 - X_2) + k_1(X_1 - X_2) + m_0(s^2X_0 - v_0) &= 0 \\ m_2(s^2X_2 - v_0) + c_2sX_2 + k_2X_2 + m_1(s^2X_1 - v_0) + m_0(s^2X_0 - v_0) &= 0 \end{aligned}$$

or, in a compact matrix form,

$$\mathbf{AX} = \mathbf{B} \tag{10.1}$$

where $\mathbf{A} = \begin{pmatrix} m_0s^2+c_0s+k_0 & -(c_0s+k_0) & 0 \\ m_0s^2 & m_1s^2+c_1s+k_1 & -(c_1s+k_1) \\ m_0s^2 & m_1s^2 & m_2s^2+c_2s+k_2 \end{pmatrix}$, $\mathbf{X} = \{X_0\ X_1\ X_2\}^T$, and $\mathbf{B} = \{v_0s\ 2v_0s\ 3v_0s\}^T$. Equation (10.1) is a set of three linear algebraic equations in $\mathbf{X}$ and thus can be solved using the matrix method. The solution set is

$$\mathbf{X} = \mathbf{A}^{-1}\mathbf{B} = \frac{\text{adj } \mathbf{A}}{\det \mathbf{A}}\ \mathbf{B}$$

or

$$\begin{pmatrix} X_0 \\ X_1 \\ X_2 \end{pmatrix} = \frac{1}{\det \mathbf{A}} \begin{pmatrix} a_{00} & a_{01} & a_{02} \\ a_{10} & a_{11} & a_{12} \\ a_{20} & a_{21} & a_{22} \end{pmatrix} \begin{pmatrix} 1 \\ 2 \\ 3 \end{pmatrix} v_0s$$

with

$$\begin{aligned}
a_{00} &= (m_1s^2+c_1s+k_1)(m_2s^2+c_2s+k_2)+m_1s^2(c_1s+k_1) \\
a_{01} &= (m_2s^2+c_2s+k_2)(c_0s+k_0) \\
a_{02} &= (c_0s+k_0)(c_1s+k_1) \\
a_{10} &= -m_0s^2(m_2s^2+c_2s+k_2) - m_0s^2(c_1s+k_1) \\
a_{11} &= (m_0s^2+c_0s+k_0)(m_2s^2+c_2s+k_2) \\
a_{12} &= (m_0s^2+c_0s+k_0)(c_1s+k_1) \\
a_{20} &= m_0m_1s^4 - m_0s^2(m_1s^2+c_1s+k_1) \\
a_{21} &= -(m_0s^2+c_0s+k_0)m_1s^2 - m_0s^2(c_0s+k_0) \\
a_{22} &= (m_0s^2+c_0s+k_0)(m_1s^2+c_1s+k_1)+m_0s^2(c_0s+k_0)
\end{aligned}$$

and

$$\begin{aligned}
\det \mathbf{A} = \ & (m_0s^2+c_0s+k_0)(m_1s^2+c_1s+k_1)(m_2s^2+c_2s+k_2) \\
& +m_0s^2(c_0s+k_0)(c_1s+k_1) + m_1s^2(c_1s+k_1)(m_0s^2+c_0s+k_0) \\
& +m_0s^2(c_0s+k_0)(m_2s^2+c_2s+k_2)
\end{aligned}$$

Then,

$$X_1(s) = \frac{a_{10}m_0 + a_{11}(m_0 + m_1) + a_{12}(m_0 + m_1 + m_2)}{\det \mathbf{A}} v_0$$

$$X_2(s) = \frac{a_{20}m_0 + a_{21}(m_0 + m_1) + a_{22}(m_0 + m_1 + m_2)}{\det \mathbf{A}} v_0$$

Since $\mathrm{L}\{\ddot{x}(t)\} = s^2X(s) - sx(0) - \dot{x}(0)$, the accelerations in the complex s domain are

$$A_1(s) = s^2X_1(s) - v_0 = \frac{v_0}{\det \mathbf{A}}[s^2a_{10}m_0 + s^2a_{11}(m_0+m_1) + s^2a_{12}(m_0+m_1+m_2) - \det \mathbf{A}]$$

$$A_2(s) = s^2X_2(s) - v_0 = \frac{v_0}{\det \mathbf{A}}[s^2a_{20}m_0 + s^2a_{21}(m_0+m_1) + s^2a_{22}(m_0+m_1+m_2) - \det \mathbf{A}]$$

After simplification,

$$\begin{aligned}
A_1(s) &= -\frac{v_0}{\det \mathbf{A}}[m_0c_1c_s^4 + (m_0k_1c_2 + m_0k_2c_1 + c_0c_1c_2)s^3 \\
&\quad + (m_1k_1k_2 + k_0c_1c_2 + k_1c_0c_2 + k_2c_0c_1)s^2 \\
&\quad + (k_0k_1c_2 + k_0k_2c_1 + k_1k_2c_0)s + k_0k_1k_2] \\
A_2(s) &= -\frac{v_0}{\det \mathbf{A}}[m_0m_1c_2s^5 + m_0m_1k_2 + m_0c_1c_2 + m_1c_0c_2)s^4 \\
&\quad + (m_0k_1c_2 + m_0k_2c_0 + m_0k_2c_1 + m_0c_0c_2 + m_1k_0c_2 + m_1k_2c_0 + c_0c_1c_2)s^3 \\
&\quad + (m_0k_0k_2 + m_0k_0c_2 + m_0k_1k_2 + m_1k_0k_2 + k_0c_1c_2 + k_1c_0c_2 + k_2c_0c_1)s^2 \\
&\quad + (k_0k_1c_2 + k_0k_2c_1 + k_1k_2c_0)s + k_0k_1k_2]
\end{aligned}$$

Dividing $A_1(s)$ by $A_2(s)$ and replacing s with $j\omega$ will lead to the transmissibility function given in Figure 4.2.

11 APPENDIX B: TRIGGERING DEVICE AND DATA ACQUISITION PROGRAM

Figure 11.1 shows the circuitry of the triggering device whose function is to send a logic 0 voltage to the digital input channel of the Keithley Data Acquisition system so as to start the acquisition process. The triggering device is necessary for eliminating unwanted data before the subject has gained his normal gait.

SOFT 500 is the BASIC programming language with added features for the use of the Keithley Data Acquisition system. The following is a listing of the program written for collecting acceleration data.

```
REM THIS BASIC PROGRAM IS TO CONTROL THE KEITHLEY DATA
REM ACQUISITION BOARD TO ACQUIRE ACCELERATION DATA FROM
REM TWO ACCELEROMETERS STRAPPED AT TWO POINTS ACROSS THE
REM KNEE JOINTS
100 CLS:KEY OFF
110 DIM X(2000),Y(2000)
120 INPUT "ENTER # OF DATA POINTS:  ",N
130 CALL INIT
140 CALL IONAME'("C0",6,0,12)
150 CALL IONAME'("C1",6,1,12)
160 CALL IONAME'("DOIN",4,0)
```

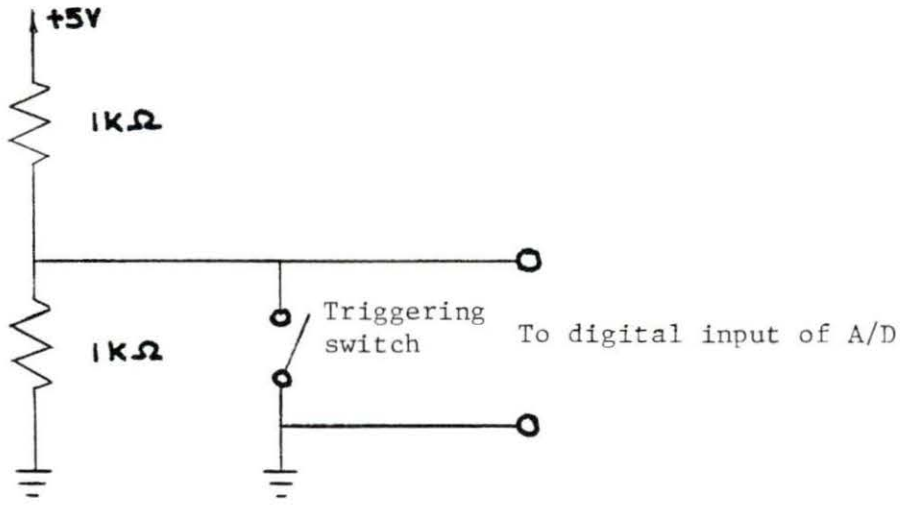

Figure 11.1: Circuit diagram of the triggering device

```
170 CALL DIGINTRIG'("DOIN","OFF")
180 CALL ANINQ'("A%",N,"C0,C1",200)
190 CALL ARGET'("A%",1.,N,"C0",1,X,0)
200 CALL ARGET'("A%",1.,N,"C1",1,Y,0)
210 SUMX=0:SUMY=0
220 FOR I=1 TO N:SUMX=SUMX+X(I):SUMY=SUMY+Y(I):NEXT
230 MEANX=SUMX/N:MEANY=SUMY/N
240 OPEN "B:lat1.DAT" FOR OUTPUT AS #1!
250 FOR I=1 TO N
260 X(I)=X(I)-MEANX:Y(I)=Y(I)-MEANY:PRINT #1,X(I),Y(I)
270 NEXT
280 CLOSE #1
290 SCREEN 2
300 FOR I=2 TO N STEP 2
310 PSET (I/2,100-10*X(I))
320 PSET (I/2,100-10*Y(I))
330 NEXT
340 I$=INKEY$:IF I$="" THEN 340
350 CLS:SCREEN 0:WIDTH 80:KEY ON
360 END
```

12 APPENDIX C: PROGRAMS FOR DATA ANALYSIS

The following FORTRAN program is the first program for data analysis. It uses HGRAPH to plot raw data in the landscape form.

```
      VIRTUAL X1(0:1024),X2(0:1024),T(0:1024)
      BYTE DATFL(14)
      NS=1024
      DT=0.002
      MRF=2
      PI=3.14159265
      DO 2 I=1,10
2        DATFL(I)=' '
      WRITE (5,4)
4     FORMAT ('$    INPUT DATA FILE NAME:  ')
      READ (7,5) DATFL
5     FORMAT (14A1)
      OPEN (UNIT=1,TYPE='OLD',NAME=datfl)
      XM=0.
      DO 10,I=0,NS-1
         READ (1,*) X1(I),X2(I)
         X1(I)=10.*X1(I)
         X2(I)=10.*X2(I)
         T(I)=DT*I
         IF(X1(I).GT.XM) XM=X1(I)
10    CONTINUE
      CLOSE (UNIT=1)
      TOP=INT(XM)+1
```

```
      RIGHT=T(NS-1)
      CALL INIPLT(99,10.,7.)
      CALL FRAME(0.,10.,4.0,7.)
      CALL WINDOW(1.8,8.8,0.1,2.0)
      CALL SCALE(0.,RIGHT,-TOP,TOP)
      CALL AXIS(RIGHT/4.,TOP/2.,' ',1,1,2,
     1  'ACCELERATION (m/s)',18,1,0)
      CALL VDASHLN(T,X1,NS,0,0,1,0,0)
      CALL FRAME(0.,10.,0.,4.0)
      CALL WINDOW(1.8,8.8,1.6,3.5)
      CALL AXIS(RIGHT/4.,TOP/2.,'TIME (Seconds)',14,1,2,
     1  'ACCELERATION (m/s)',18,1,0)
      CALL VDASHLN(T,X2,NS,0,0,1,0,0)
      CALL ENDPLT
      STOP
      END
```

The following program low-pass filters the signals and plots the filtered version.

```
      VIRTUAL X1(0:1024),X2(0:1024),Y1(0:1024),Y2(0:1024)
      BYTE IN(14)
      BYTE OUT(14)
      N=1024
      DO 2 I=1,10
2        IN(I)=' '
      WRITE (5,4)
4     FORMAT ('$     INPUT DATA FILE NAME:  ')
      READ (7,5) IN
5     FORMAT (14A1)
      DO 12 I=1,10
12       OUT(I)=' '
      OPEN (UNIT=1,TYPE='OLD',NAME=in)
      READ (1,*) (X1(I),X2(I),I=0,N-1)
      CLOSE(UNIT=1)
      Y1(0)=X1(0)
      Y1(1)=X1(1)
```

```
      Y1(2)=X1(2)
      Y2(0)=X2(0)
      Y2(1)=X2(1)
      Y2(2)=X2(2)
      DO 20 I=3,N-1
         Y1(I)=1.162*Y1(I-1)-0.696*Y1(I-2)+0.138*Y1(I-3)
     1          +0.049*(X1(I)+3.*X1(I-1)+3.*X1(I-2)+X1(I-3))
         Y2(I)=1.162*Y2(I-1)-0.696*Y2(I-2)+0.138*Y2(I-3)
     2          +0.049*(X2(I)+3.*X2(I-1)+3.*X2(I-2)+X2(I-3))
20    CONTINUE

      WRITE (5,14)
14    FORMAT ('$    OUTPUT DATA FILE NAME:  ')
      READ (7,15) OUT
15    FORMAT (14A1)
      OPEN (UNIT=2,TYPE='NEW',NAME=out)
      DO 30 I=0,N-1
      WRITE (2,*) Y1(I),Y2(I)
30    CONTINUE
      CLOSE (UNIT=2)
      STOP
      END
```

The following FORTRAN program first computes crosscorrelation of the signals, squares-windows the signals, and subtracts from the signals the linear regressions on time. It then subjects the resulting series to a Hanning window, performs FFT, calculates transmissibility function, and plots the results.

```
      VIRTUAL X1(0:1024),X2(0:1024),T(0:128)
      COMMON DT,MRF,PI,XM,RIGHT
      BYTE DATFL(14)
      NS=1024
      DT=0.002
      MRF=4
```

```
      PI=3.14159265
      DO 2 I=1,10
2        DATFL(I)=' '
      WRITE (5,4)
4     FORMAT ('$    INPUT DATA FILE NAME:  ')
      READ (7,5) DATFL
5     FORMAT (14A1)
      OPEN (UNIT=1,TYPE='OLD',NAME=datfl)
      READ (1,*) (X2(I),X1(I),I=0,NS-1)
      CLOSE(UNIT=1)
      XM=0.
      DO 20 I=NS/2,NS-1
         IF(X1(I).GT.XM) THEN
           XM=X1(I)
           IM=I
         ELSE
           GO TO 20
         END IF
20    CONTINUE
      XM=10.*XM
      NS=128
      DO 30 I=0,NS-1
         X1(I)=10.*X1(IM-30+I)
         X2(I)=10.*X2(IM-30+I)
         T(I)=DT*I*1000.
30    CONTINUE
      CALL CROSS(X1,X2,NS,T)
      CALL WAVE(X1,X2,NS,T)
      CALL FFTPLT(X1,X2,NS,N)
      STOP
      END

      SUBROUTINE WAVE(X1,X2,NS,T)
      VIRTUAL X1(0:128),X2(0:128),T(0:128),W(0:128)
      COMMON DT,MRF,PI,XM,RIGHT
      TOP=INT(XM)+1
      RIGHT=T(NS-1)
      CALL INIPLT(99,7.,10.)
      CALL FRAME(0.,7.,5.,10.)
```

```
      CALL WINDOW(1.7,5.7,1.6,3.8)
      CALL SCALE(0.,RIGHT,-TOP,TOP)
      CALL AXIS(RIGHT/4.,TOP/2.,'TIME (Millisec)',15,1,0,
     1  'ACCELERATION (m/s*s)',20,1,0)
      CALL VDASHLN(T,X1,NS,0,0,1,0,0)
      CALL VDASHLN(T,X2,NS,0,0,1,0,2)
      CALL LR(X1,NS)
      CALL LR(X2,NS)
      DO 10 I=0,NS-1
         W(I)=(SIN(3.1415926*I/(NS-1)))**2
         X1(I)=X1(I)*W(I)
         X2(I)=X2(I)*W(I)
10    CONTINUE
      CALL FRAME(0.,7.,0.,5.)
      CALL WINDOW(1.7,5.7,2.4,4.6)
      CALL AXIS(RIGHT/4.,TOP/2.,'TIME (Millisec)',15,1,0,
     1  'ACCELERATION (m/s*s)',20,1,0)
      CALL VDASHLN(T,X1,NS,0,0,1,0,0)
      CALL VDASHLN(T,X2,NS,0,0,1,0,2)
      CALL ENDPLT
      RETURN
      END

      SUBROUTINE LR(Y,N)
      VIRTUAL X(0:128),Z(0:128),Y(0:128)
      SX=0.0
      SY=0.0
      SXY=0.0
      SXS=0.0
      DO 10 I=0,N-1
         X(I)=FLOAT(I)
         SX=SX+X(I)
         SY=SY+Y(I)
         SXY=SXY+X(I)*Y(I)
         SXS=SXS+X(I)**2
10    CONTINUE
      FN=FLOAT(N)
      A=(FN*SXY-SY*SX)/(FN*SXS-SX**2)
      B=(SY-A*SX)/FN
```

```
      DO 20 I=0,N-1
         Z(I)=A*X(I)+B
         Y(I)=Y(I)-Z(I)
20    CONTINUE
      RETURN
      END

      SUBROUTINE CROSS(X1,X2,NS,T)
      VIRTUAL X1(0:128),X2(0:128),T(0:128),R(0:128)
      COMMON DT,MRF,PI,XM,RIGHT
      CALL CORR(X1,X1,NS,R)
      RX1=R(0)
      CALL CORR(X2,X2,NS,R)
      RX2=R(0)
      CALL CORR(X1,X2,NS,R)
      DO 15 I=0,NS/4
         R(I)=R(I)/SQRT(RX1*RX2)
15    CONTINUE
      CALL INIPLT(99,7.,10.)
      CALL FRAME(0.,7.,5.,10.)
      CALL WINDOW(1.7,5.7,1.6,3.8)
      CALL SCALE(0.,32.,-1.,1.)
      CALL AXIS(4.,1.,'TIME (Millisec)',15,1,0,
     1 'CROSSCORRELATION',16,1,0)
      CALL VDASHLN(T,R,NS/4,0,0,1,0,0)
      CALL ENDPLT
      RETURN
      END

      SUBROUTINE CORR(X,Y,N,R)
      VIRTUAL X(0:128),Y(0:128),R(0:128)
      DO 10 I=0,N-1
         R(I)=0.0
         DO 20 K=0,N-1-I
            R(I)=R(I)+X(K)*Y(K+I)
20       CONTINUE
         R(I)=R(I)/N
10    CONTINUE
      RETURN
```

```
      END

      SUBROUTINE FFT(X,NS,N,Y)
      VIRTUAL X(0:1024)
      COMPLEX Y(0:1024),U,W,T
      COMMON DT,MRF,PI
      DO 2 K=1,10
         IF(NS.LE.2**K) GO TO 3
2     CONTINUE
3     DO 5 I=1,NS
         Y(I)=CMPLX(X(I-1),0.)
5     CONTINUE
      DO 6 I=NS+1,2**K*MRF
6        Y(I)=CMPLX(0.,0.)
      N=2**K*MRF
      M=IFIX(ALOG10(FLOAT(N))/ALOG10(2.))
      DO 20 L=1,M
      LE=2**(M+1-L)
      LE1=LE/2
      U=(1.0,0.0)
      W=CMPLX(COS(PI/FLOAT(LE1)),-SIN(PI/FLOAT(LE1)))
      DO 20 J=1,LE1
      DO 10 I=J,N,LE
      IP=I+LE1
      T=Y(I)+Y(IP)
      Y(IP)=(Y(I)-Y(IP))*U
10    Y(I)=T
20    U=U*W
      NV2=N/2
      NM1=N-1
      J=1
      DO 30 I=1,NM1
      IF(I.GE.J) GO TO 25
      T=Y(J)
      Y(J)=Y(I)
      Y(I)=T
25    K=NV2
26    IF(K.GE.J) GO TO 30
      J=J-K
```

```
      K=K/2
      GO TO 26
30    J=J+K
      RETURN
      END

      SUBROUTINE FFTPLT(X1,X2,NS,N)
      VIRTUAL X1(0:1024),X2(0:1024),X(0:1024),F(0:1024)
      VIRTUAL PHSE1(0:1042),PHSE2(0:1042),PHSE(0:1024)
      COMPLEX Y1(0:1024),Y2(0:1024),T1,T2
      COMMON DT,MRF,PI
      CALL FFT(X1,NS,N,Y1)
      CALL FFT(X2,NS,N,Y2)
      NN=N/2-1
      XMAX=1.0
      DO 5 I=0,NN
         F(I)=I/(N*DT)
         T1=Y1(I+1)
         T2=Y2(I+1)
         X1(I)=CABS(T1)
         X2(I)=CABS(T2)
         X(I)=X2(I)/X1(I)
         PHSE1(I)=57.29578*(ATAN2(AIMAG(T1),REAL(T1)))
         PHSE2(I)=57.29578*(ATAN2(AIMAG(T2),REAL(T2)))
         PHSE(I)=PHSE2(I)-PHSE1(I)
         IF(X1(I).GT.XMAX) XMAX=X1(I)
5     CONTINUE
      DO 10 I=0,NN
         X1(I)=X1(I)/XMAX
         X2(I)=X2(I)/XMAX
10    CONTINUE
      RIGHT=F(NN)/4.
      CALL INIPLT(99,7.,10.)
      CALL FRAME(0.,7.,5.,10.)
      CALL WINDOW(1.7,5.7,1.6,3.8)
      CALL SCALE(0.,RIGHT,0.,1.5)
      CALL AXIS(RIGHT/4,.5,'FREQUENCY (Hertz)',17,1,0,
     1 'NORMALIZED MAGNITUDE',20,1,1)
      CALL VDASHLN(F,X1,NN,0,0,1,0,0)
```

```
 CALL VDASHLN(F,X2,NN,0,0,1,0,2)
 CALL FRAME(0.,7.,0.,5.)
 CALL WINDOW(1.7,5.7,2.4,4.6)
 CALL SCALE(0.,RIGHT,-180.,180.)
 CALL AXIS(RIGHT/4,90.,'FREQUENCY (Hertz)',17,1,0,
1  'PHASE (Degrees)',15,1,0)
 CALL VDASHLN(F,PHSE1,NN,0,0,1,0,0)
 CALL VDASHLN(F,PHSE2,NN,0,0,1,0,2)
 CALL ENDPLT
 CALL INIPLT(99,7.,10.)
 CALL FRAME(0.,7.,5.,10.)
 CALL WINDOW(1.7,5.7,1.6,3.8)
 CALL SCALE(0.,RIGHT,0.,5.)
 CALL AXIS(RIGHT/4,2.5,'FREQUENCY (Hertz)',17,1,0,
1 'MAGNITUDE',9,1,1)
 CALL VDASHLN(F,X,NN,0,0,1,0,0)
 CALL FRAME(0.,7.,0.,5.)
 CALL WINDOW(1.7,5.7,2.4,4.6)
 CALL SCALE(0.,RIGHT,-360.,360.)
 CALL AXIS(RIGHT/4,180.,'FREQUENCY (Hertz)',17,1,0,
1  'PHASE (Degrees)',15,1,0)
 CALL VDASHLN(F,PHSE,NN,0,0,1,0,0)
 CALL ENDPLT
 RETURN
 END
```

13 APPENDIX D: PROGRAM TO AID IN DESIGN OF DIGITAL BUTTERWORTH FILTERS

One of the advantages of a digital Butterworth filter over its analog counterpart is that the designer has precise control over the cut-off frequency and the roll-off rate of the filter. Yet, the algebra involved in designing high-order digital filters is very tedious. The following FORTRAN program for design of low-pass filters is the implementation of a program from Stanley and Dougherty (1984). The program assumes no filter design knowledge of the user. It asks the user to type in the order and cut-off frequency of the desired filter and the sampling rate of the A/D converter. It then prints the calculated coefficients of both the numerator and the denominator of the filter function. If a high-pass, band-pass, or a notch filter is in order, a simple frequency transformation will lead to the desired filter (Jackson, 1986).

```
C     THIS PROGRAM (LPF.FOR) IS TO OBTAIN COEFFICIENTS OF
C     BOTH THE NUMERATOR AND DENOMINATOR OF THE STABLE
C     BUTTERWORTH DIGITAL LOW-PASS FILTER.  IT ALSO USES
C     THE HGRAPH TO PLOT THE FREQUENCY RESPONSE OF THE RESULTING
C     FILTER.
```

```
      REAL X(0:20)
      NN=512
      CALL BUTTER(X,N,FS)
      CALL PLTLP(X,N,NN,FS)
      STOP
      END

      SUBROUTINE BUTTER(X,N,FS)
      REAL X(0:20),Y(0:20),U(0:20),V(0:20)
      PI=3.141592654
      WRITE(7,10)
10    FORMAT(//,12X,'ENTER N (INTEGER), # OF DEGREES OF DENOMINATOR
     1  OF FILTER H(Z)')
      READ(5,20) N
      WRITE(1,20) N
20    FORMAT(I)
      M=2*N
      RN=FLOAT(N)
      WRITE(7,30)
30    FORMAT(//,12X,'ENTER FC (REAL), CUTOFF FREQUENCY IN HERTZ')
     READ(5,40) FC
40    FORMAT(F)
      WC=2*PI*FC
      WRITE(7,50)
50    FORMAT(//,12X,'ENTER FS (REAL), SAMPLING FREQUENCY IN HERTZ')
      READ(5,40) FS
      T=1./FS
      A=SIN(WC*T/2)/COS(WC*T/2)
      LO=MOD(N,2)
      IF(LO.EQ.1) GO TO 200
      DO 110 I=1,M
      X(I)=A*COS((2.*FLOAT(I-1)+1.)*PI/(2.*RN))
      Y(I)=A*SIN((2.*FLOAT(I-1)+1.)*PI/(2.*RN))
110   CONTINUE
      GO TO 300
200   DO 210 I=1,M
      X(I)=A*COS(FLOAT(I-1)*PI/RN)
      Y(I)=A*SIN(FLOAT(I-1)*PI/RN)
210   CONTINUE
```

```
300 PRINT 320
    DO 310 I=1,M
    U(I)=(1.-X(I)**2-Y(I)**2)/((1.-X(I))**2+Y(I)**2)
    V(I)=2.*Y(I)/((1.-X(I))**2+Y(I)**2)
    K=I-1
    PRINT 330, K,U(I),Y(I)
310 CONTINUE
    PRINT 315, FC
315 FORMAT(//,15X,'CUTOFF FREQUENCY IS :',F7.2,' HERTZ',/)
320 FORMAT(//,10X,'POLE LOCATIONS OF H(Z)*H(1/Z) IN 1/Z-PLANE',
   1 //,22X,'REAL PART',11X,'IMAG PART',//)
330 FORMAT(12X,I3,3X,E17.8,3X,E17.8)
    CALL ZERO(X,1,N+1)
    CALL ZERO(Y,1,N+1)
    L=0
    DO 400 I=1,M
    II=I
    J=1
410 IF((X(J).NE.U(I)).OR.(ABS(Y(J)).NE.ABS(V(I)))) GO TO 420
    IF(J.EQ.II) GO TO 400
    J=J+1
    GO TO 410
420 L=L+1
    X(L)=U(I)
    Y(L)=V(I)
400 CONTINUE
    L=0
    DO 430 I=1,N+1
    R=X(I)**2+Y(I)**2
    IF(R.LE.1.) GO TO 430
    L=L+1
    X(L)=X(I)/R
    Y(L)=-Y(I)/R
430 CONTINUE
    IF(LO.EQ.0) GO TO 500
    MAX=N/2+1
    DO 440 I=1,MAX
    IF(ABS(Y(I)).GT.10.E-6) GO TO 440
    INDEX=I
```

```
440 CONTINUE
    RX=X(INDEX)
    DO 450 I=INDEX,MAX-1
    X(I)=X(I+1)
    Y(I)=Y(I+1)
450 CONTINUE
500 CONTINUE
    NN=N/2
    DO 510 I=1,NN
    U(I)=-2.*X(I)
    V(I)=X(I)**2+Y(I)**2
510 CONTINUE
    CALL REALCO(NN,X,Y,U,V)
    IF(LO.EQ.0) GO TO 530
    IF(NN.NE.1) GO TO 529
    Y(2)=X(2)
    Y(3)=X(3)
529 CONTINUE
    Y(1)=1.
    DO 520 I=2,N+1
    X(I)=X(I)-Y(I-1)*RX
520 CONTINUE
530 CONTINUE
    PRINT 540
540 FORMAT(//,10X,'COEFFICIENTS OF DENOMINATOR IN Z, NOT IN 1/Z',
   1 /,10X,'STARTING FROM THE HIGHEST DEGREE COEFFICIENT',//)
    PRINT 550, ((I,X(I)),I=1,N+1)
550 FORMAT(12X,I3,3X,E17.8)
    RETURN
    END

    SUBROUTINE REALCO(NN,X,Y,U,V)
    REAL X(0:20),Y(0:20),U(0:20),V(0:20)
    CALL ZERO(X,1,20)
    CALL ZERO(Y,1,20)
    X(1)=1.
    X(2)=U(1)
    X(3)=V(1)
    IF(NN.EQ.1) RETURN
```

```
    M=2
100 MM=2*M+1
    DO 110 I=2,MM
    II=I
    IF(II.EQ.2) GO TO 111
    Y(I)=X(I)+X(I-1)*U(M)+X(I-2)*V(M)
    GO TO 110
111 Y(I)=X(I)+U(M)
110 CONTINUE
    DO 120 I=2,MM
    X(I)=Y(I)
120 CONTINUE
    IF(M.EQ.NN) RETURN
    M=M+1
    GO TO 100
    END

    SUBROUTINE ZERO(A,K,L)
    REAL A(0:20)
    DO 10 I=K,L
10  A(I)=0.0
    RETURN
    END

    SUBROUTINE PLTLP(X,N,NN,FS)
    COMPLEX Z(0:512),XN,XD,H
    REAL X(0:20),F(0:512),AMP(0:512),PHSE(0:512),K
    DO 10 I=0,NN-1
       F(I)=(I*FS)/NN
       WT=6.283/NN*I
       Z(I)=CMPLX(COS(WT),SIN(WT))
       XN=(1.+Z(I))**N
       XD=(0.,0.)
       DO 15 J=1,N+1
          XD=XD+X(J)*Z(I)**(N-J+1)
15     CONTINUE
       IF(I.GT.0) GO TO 14
       K=CABS(XD/XN)
       PRINT 13, K
```

```
13      FORMAT(//,15X,'K =',F15.8)
14      H=K*(XN/XD)
        AMP(I)=CABS(H)
        PHSE(I)=57.29578*(ATAN2(AIMAG(H),REAL(H)))
10    CONTINUE
      RIGHT=FS/2.
      CALL INIPLT(99,7.,10.)
      CALL FRAME(0.,7.,6.,10.)
      CALL WINDOW(1.7,5.7,.2,2.7)
      CALL SCALE(0.,RIGHT,0.,1.5)
      CALL AXIS(RIGHT/2.,.5,' ',1,1,0,'MAGNITUDE',9,1,1)
      CALL DASHLN(F,AMP,NN,0,0,1,0,0)
      CALL FRAME(0.,7.,1.,6.)
      CALL WINDOW(1.7,5.7,2.,4.5)
      CALL SCALE(0.,RIGHT,-180.,180.)
      CALL AXIS(RIGHT/2.,90.,'FREQUENCY (Hertz)',17,1,1,
     1  'PHASE (Degrees)',15,1,0)
      CALL DASHLN(F,PHSE,NN,0,0,1,0,0)
      CALL ENDPLT
      RETURN
      END
```

In this sample low-pass filter design, the cut-off frequency is 75 Hertz, order of the filter three, and sampling frequency 500 Hertz. The resulting filter function is

$$H(z) = 0.049\frac{(z+1)^3}{z^3 - 1.162z^2 + 0.696z - 0.138}$$

whose magnitude and phase plots are shown in Figure 13.1.

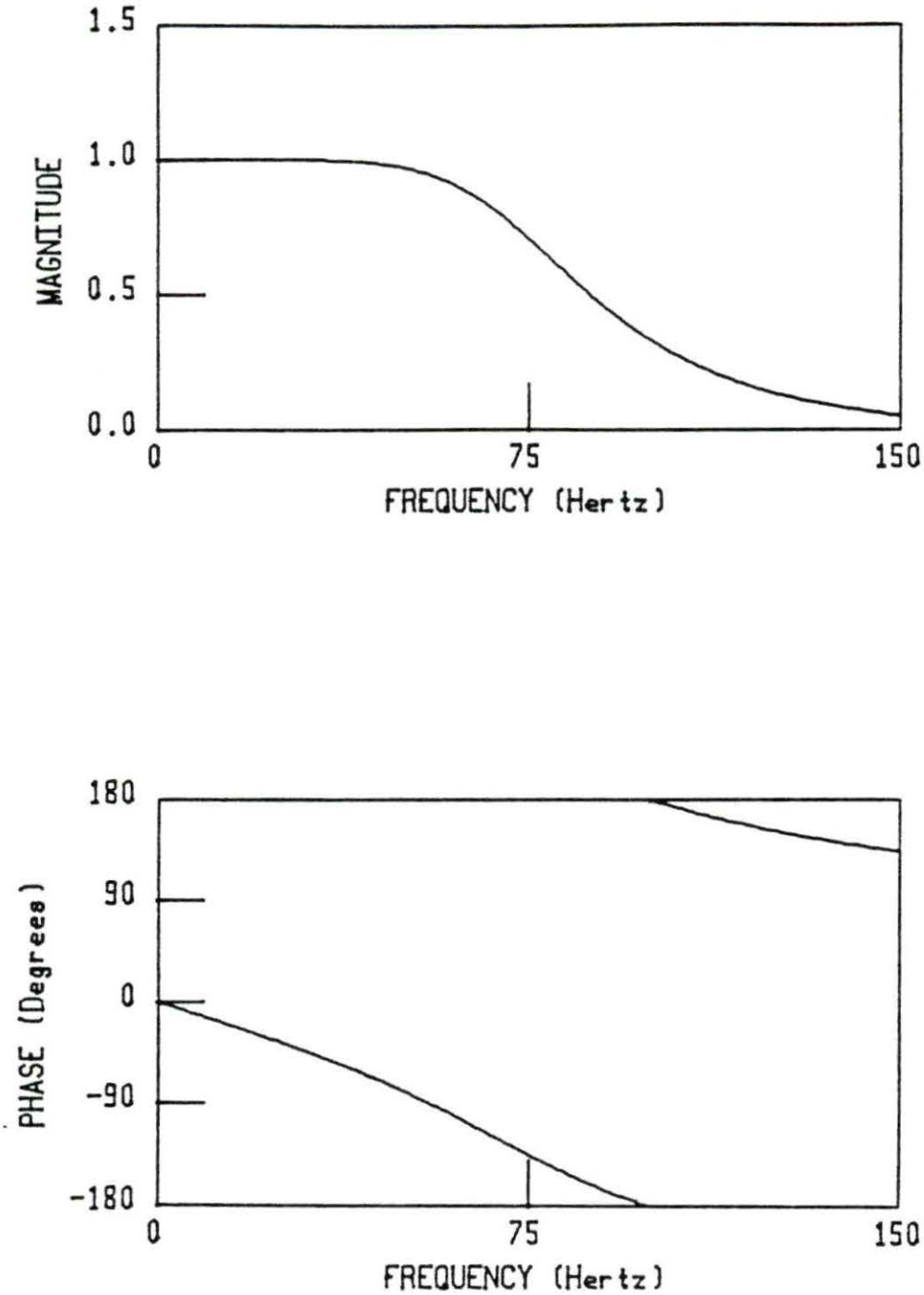

Figure 13.1: Magnitude and phase plots of a low-pass filter design

14 APPENDIX E: ZERO-PADDING AND SAMPLE OUTPUT OF THE FFT SUBROUTINE

Zero padding refers to the operation of extending a time series of length N_1 to a length $N_2 > N_1$ by appending $N_2 - N_1$ zero values to the given series so that the density of DFT is increased (Jackson, 1986; Oppenheim and Schafer, 1975; Russell, 1978). For example, if

$$x(i) = \{x_0\ x_1\ x_2\ \cdots\ x_i\ \cdots\ x_{N_1}\}$$

the zero-padded series will be

$$y(i) = \{x_0\ x_1\ \cdots\ x_i\ \cdots\ x_{N_1}\ \overbrace{0\ 0\ \cdots\ 0\ 0}^{N_2-N_1}\}$$

When DFT is performed on the expanded series, $N_2 - N_1$ more DFT samples will be generated, an increase in resolution. As an example, Figure 14.1 shows the FFT magnitude and the phase plots of an time series of N_1 with no zero-padding, and Figure 14.2 displays the FFT magnitude and phase plots of the same time series zero-padded with $N_2 - N_1 = 3N_1$. The frequency resolution of the latter was increased dramatically.

It is important, when doing digital Fourier transformation, to check and see if the FFT routine to be used functions correctly. The FFT routine for this project was

copied from Oppenheim and Schafer (1975) and was tested using different known functions. Figure 14.3 gives one set of sample test plots. The first one shows the plot of a unit square time function with a window size of $\tau = 0.08$ second, and the second and the third show the FFT magnitude and phase plots of the unit square function. For a quick check, the frequency at which the magnitude of the FFT has its first zero value should be $f = \frac{1}{\tau} = 12.5$ Hertz.

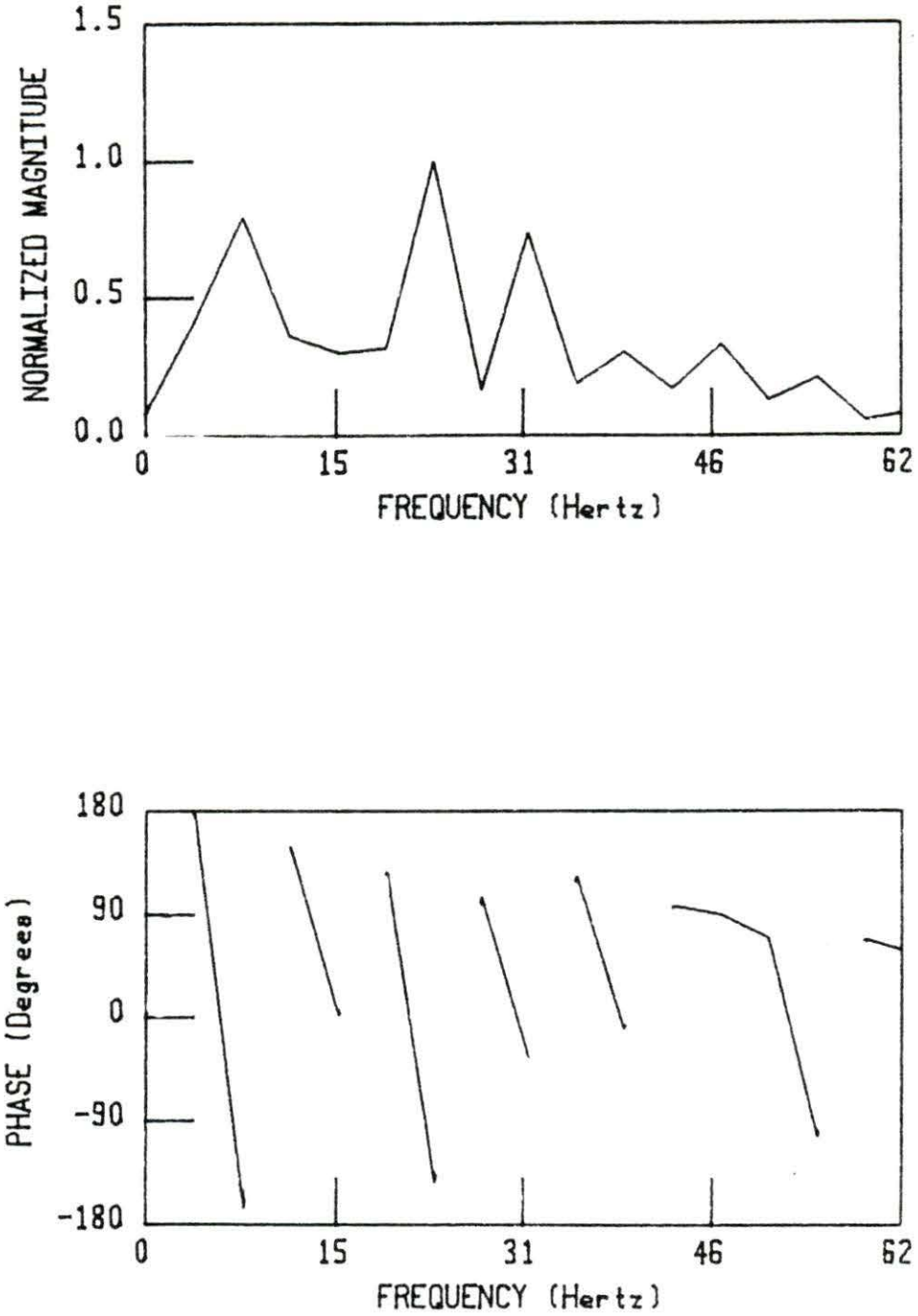

Figure 14.1: FFT of a time series with no zero-padding

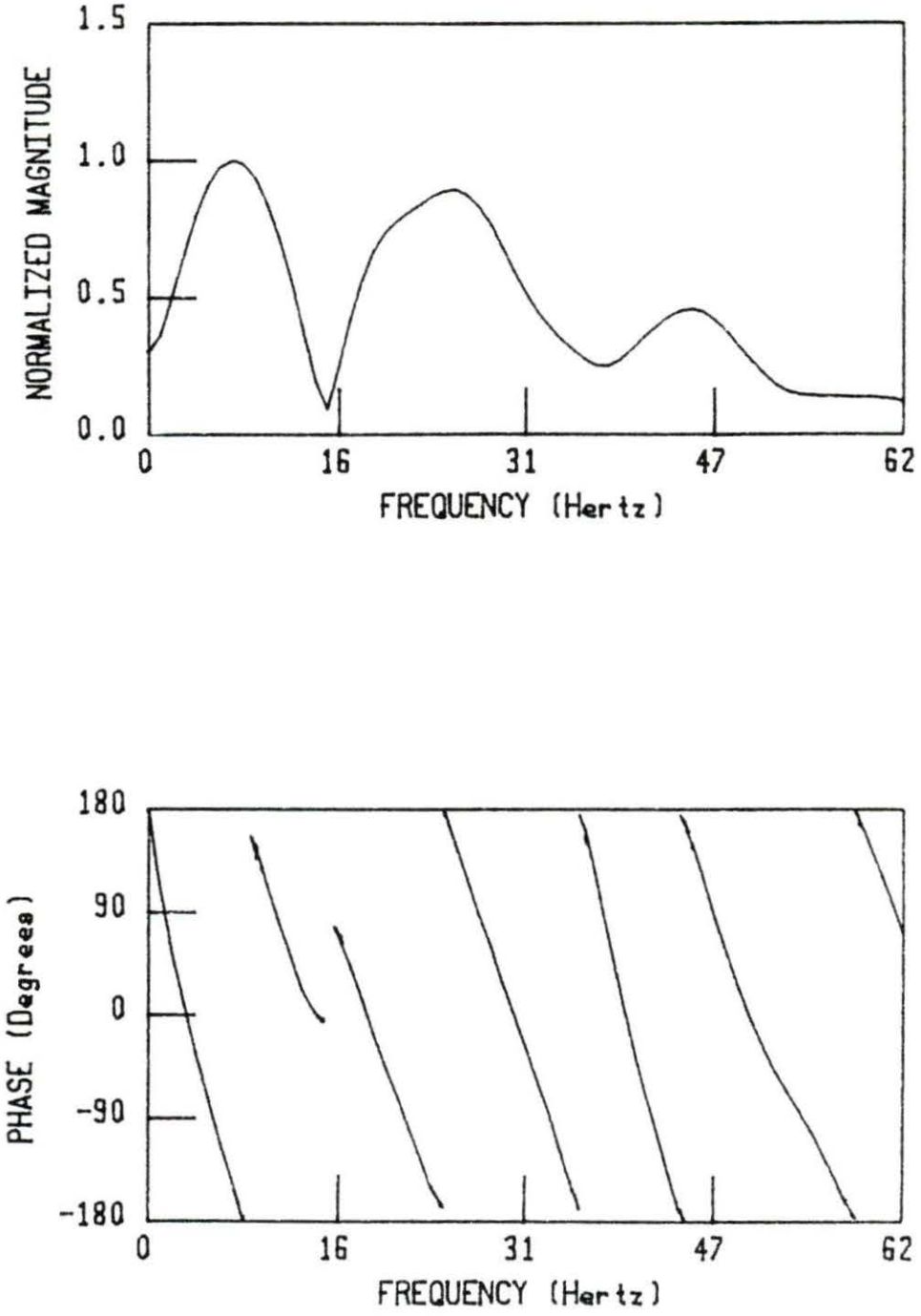

Figure 14.2: FFT of the same time series with zero-padding